

Regression-based projection for learning Mori–Zwanzig operators

Yen Ting Lin^{1,†,*}, Yifeng Tian^{1,2,†}, and Daniel Livescu²

¹*Information Sciences Group, Computer, Computational and Statistical Sciences Division (CCS-3), Los Alamos National Laboratory, Los Alamos, NM 87545, USA*

²*Computational Physics and Methods Group, Computer, Computational and Statistical Sciences Division (CCS-2), Los Alamos National Laboratory, Los Alamos, NM 87545, USA*

[†]*These authors contributed equally.*

^{*}*Corresponding author: yentingl@lanl.gov*

May 12, 2022

Abstract

We propose to adopt statistical regression as the projection operator to enable data-driven learning of the operators in the Mori–Zwanzig formalism. We present a principled algorithm to extract the Markov and memory operators for any regression models. We show that the choice of linear regression results in a recently proposed data-driven learning algorithm based on Mori’s projection operator, which can be considered as a higher-order approximate Koopman learning method. We show that more expressive, potentially nonlinear regression models naturally fill in the gap between the highly idealized and computationally efficient Mori’s projection operator and the most optimal yet computationally infeasible Zwanzig projection operator. We performed numerical experiments and extracted the operators for an array of regression-based projections, including linear, polynomial, spline, and neural-network-based regression, showing a progressive improvement as the complexity of the regression model increased. Our proposition provides a general framework to extract memory-dependent corrections and can be readily applied to an array of data-driven learning methods for stationary dynamical systems in the literature.

Keywords: Mori–Zwanzig formalism, Koopman representation, nonlinear projection operators, data-driven learning, regression, neural networks

AMS subject classifications: 37M19, 37M99, 46N55, 65P99, 82C31

1 Introduction

More than half a century ago, Mori [1] and Zwanzig [2] developed a mathematically rigorous formalism for constructing reduced-order models for dynamical systems with many degrees

of freedom. In the context of non-equilibrium statistical mechanics, the typical number of the degrees of the freedom is of the order of Avogadro's number. In contrast to tracking the dynamics of each degree of freedom, reduced-order models (also referred to as the coarse-grained models in the context of statistical physics) describe the dynamics of a relatively small number of variables that are of our interests. In the lingo of model coarse-graining, this set of dynamic variables is referred to as the “resolved variables”, and the rest degrees of freedom in the system is referred to as the “under-resolved” ones. Reduced-order models are particularly useful in describing the emergent physics at the mesoscopic or macroscopic scales. They are also more computationally efficient to simulate, and thus play an essential role in bridging multi-scale models.

The key difficulty in constructing a reduced-order model is the closure problem: we must quantify the effect of the under-resolved variables on the resolved ones before we can prescribe a closed evolutionary equation for the resolved dynamic variables. To solve the closure problem, Mori and Zwanzig adopted an elegant projection operator approach. Formally, a projection operator maps a function of both resolved and under-resolved variables to a function that only depends on the resolved ones. Mori–Zwanzig formalism is a mathematical procedure which prescribes exact results, that the resulting reduced-order dynamics generally depends on its past history. In addition, the Mori–Zwanzig memory effect quantifies the interactions between the resolved and under-resolved dynamics, and the effect critically depends on the choice of the resolved variables and the projection operators.

Theoretically speaking, there are infinitely many choices of the projection operators. In the literature, the commonly chosen projections include (1) Mori's linear projection [1], (2) finite-rank projection operator, which is essentially Mori's projection operator with a proper ortho-normalization, and (3) Zwanzig's fully nonlinear projection [2, 3]. Several recent studies established that it is possible to adopt a data-driven approach to learn the Mori–Zwanzig operators using simulation data, if the projection operator is Mori's linear projection operator [4, 5, 6, 7, 8, 9, 10]. In addition, we also showed that our previously proposed algorithms [9] provide higher-order and memory-dependent corrections to existing data-driven learning of the approximate Koopman operators [11, 12, 13, 14].

Despite of being a consistent theoretical framework to the approximate Koopman learning, Mori's projection operator is greatly limited by its linear nature. That is, after the projection, all functions must be expressed as linear combinations of a set of resolved variables which are specified *a priori*. As such, despite the fact that data-driven Mori–Zwanzig framework ensures an accurate prediction of the projected dynamics, its utility still critically depends on the choice of the set of resolved variables, which serves as linear bases functions of the projected functional space. To the authors' best knowledge, there is no principled way to select the set of functions for linearly spanning the optimal subspace for general dynamical systems. With a non-optimal choice of the set of functions, the difference between the accurately predicted projected dynamics and the true dynamics can be very large [9]. The same problem also manifests itself in the approximate Koopman learning framework [14]. Furthermore, Mori's projection operator is not compatible with many nonlinear closure schemes [15, 16]. Neither can we generalize the Mori's restrictive linear projection operator to methods based on machine learning (ML) [17, 18, 19, 20]. In these approaches, one relies on the ML, e.g. neural networks (NNs), for identifying nonlinear relationship between the independent variables (what we know at the present) and the dependent ones (what we

want to predict in the future). With Mori’s projection operator, our data-driven learning framework [9] cannot be generalized to capture these built-in and flexible nonlinearities that are informed and constrained by data in these ML-based approaches.

At the other end of the spectrum is the Zwanzig’s fully nonlinear projection operator [2, 3] which uses conditional expectation as a projection operator. Although projection operator based on the conditional expectation is the most optimal projection operator [3], in practice, it is challenging to estimate the conditional expectations with a finite set of data, especially for those under-resolved systems in high dimensions.

To address the aforementioned difficulties, we propose to adopt general regression as a projection operator to bridge the gap between the linear Mori’s projection operator and the fully nonlinear Zwanzig projection operator. We will show that when the regression is linear, the regression-based projection operator converges to our recent result of data-driven methods for Mori’s projection operator [9]. Thus, the method we propose here is a superset of the previously published algorithms [9]. The regression-based projection has the capability to incorporate flexible nonlinear functions that are adaptable to the data. As such, our proposed formulation is most natural mathematical formulation for ML-based methods.

In addition to the theoretical formulation, we also present numerical evidence of the approach using various nonlinear regression models, including ridge regression, fully-connected neural networks (FCNN), and convolutional neural networks (CNN). On the one hand, we will show that the nonlinear regression-based projectors out-perform the linear Mori’s projector in all the systems we investigated. As such, the method that we propose in this paper can be considered as a better replacement of our recently proposed algorithms [9]. On the other hand, we will show that the predictions of the nonlinear regression-based analysis will be improved by incorporating the memory contributions prescribed by the Mori–Zwanzig formalism. As such, our proposed method is a superset of existing ML-based data-driven learning methods [17, 18, 19, 20].

2 Results

2.1 Theoretical Analysis

Full dynamical systems. Following the notation in [9], we consider an autonomous and deterministic dynamical system in \mathbb{R}^D following a continuous-time evolutionary equation

$$\frac{d}{dt}\phi(t) = \mathbf{R}(\phi(t)), \quad (1)$$

where ϕ is the state in the phase space \mathbb{R}^D and $\mathbf{R} : \mathbb{R}^D \rightarrow \mathbb{R}^D$ is the flow of the system. We will assume that the flow \mathbf{R} is locally Lipschitz throughout the state space \mathbb{R}^D , so a unique $\phi(t) \forall t \geq 0$ is ensured. We will denote the solution of (1) with the initial condition $\phi_0 \in \mathbb{R}^D$ by $\phi(t; \phi_0)$.

Observables. In reduced-order modeling, we aim to prescribe the dynamical equations for $M < D$ real-valued functions of the state variable ϕ , $g_i : \mathbb{R}^D \rightarrow \mathbb{R}$, $i = 1 \dots M$. We will exclusively consider real-valued functions but the theory can be straightforwardly generalized to complex-valued functions. We will refer to these functions as the observables, noting that observables are also referred to as descriptors or dynamic variables in other contexts, such

as in material science or statistical mechanics. We refer to an “observation” at time t as applying the set of observables to the system’s state $\phi(t; \phi_0)$, that is, $\{g_i(\phi(t; \phi_0))\}_{i=1}^M$. We remark that one can define an observable π_i to extract the i^{th} component of the state ϕ (that is, $\pi(\phi) = \phi_i$ [21]). In general, observables g must be measurable functions of the full state ϕ against some chosen distribution; see below section “A chosen distribution”.

Discrete-time snapshot data. Throughout this study, we assume that the full system has been simulated and observed at discrete times, and the observations form a data set for learning the Mori–Zwanzig operators. Specifically, we rely on samples drawn from a chosen initial distribution μ to collect the statistics of the under-resolved information. The full system is prepared at $N \gg 1$ independently and identically sampled $\phi_0^{[i]} \sim \mu$, $i = 1 \dots N$. The system is then simulated and the values of the observables are measured at uniformly distributed discrete times $k\Delta$, $k = 1 \dots K$. We refer to these observations as the *snapshots*. Without loss of generality, we will assume $\Delta = 1$ by choosing an appropriate unit of time. The full discrete-time observations thus forms an $N \times M \times K$ data matrix \mathbf{D} , such that the (i, j, k) entry of the matrix is $g_j(\phi(k-1; \phi_0^{[i]}))$. For ergodic systems, it is desirable to bypass sampling from a pre-specified initial distribution and use the distribution along a long trajectory instead. In this case, we generate a single but long trajectory from a randomly selected initial condition ϕ_0^{rand} . After the initial transient time t_c , we made $K + N$ observations every $\Delta = 1$ time. We will use these $K + N$ observation for informing the statistics from the ergodic measure. The data matrix \mathbf{D} in this case is defined as an $N \times M \times K$ matrix whose (i, j, k) entry is $g_j(\phi(t_c + i + k - 1; \phi(t_c + i - 1; \phi_0^r)))$.

Discrete-time dynamical systems. To match to the discrete-time snapshot data, we re-write the evolutionary equation (1) into a discrete-time form:

$$\phi(t+1) = \mathbf{F}(\phi(t)), \quad (2)$$

where $\mathbf{F} : \mathbb{R}^D \rightarrow \mathbb{R}^D$ is the discrete-time map. Locally Lipschitz condition ensures that such a mapping exists and is unique for any finite time $t \in \mathbb{Z}_{\geq 0}$. Our formulation is readily applicable to those systems whose underlying dynamic is discrete-time in nature; in those cases, we can begin with the discrete-time formulation Eq. (2), instead of Eq. (1).

A chosen “distribution” and measurable functions. We assume that the number of samples N is sufficiently large to capture the statistics of the time-dependent distribution induced by the deterministic dynamics from the initial distribution μ , i.e., the solution of the generalized Liouville equation corresponding to Eq. (1) [22]:

$$\partial_t \rho(\phi, t) = \sum_{i=1}^N \partial_{\phi_i} [\mathbf{R}_i(\phi) \rho(\phi, t)], \text{ with the initial data } \rho(\phi, 0) = \mu(\phi), \quad (3)$$

where $\mu(\phi)$ is the probability density function of the measure μ , assuming the measure μ is dominated by the Lebesgue measure $d\phi$ in the state space \mathbb{R}^D . When using the single trajectory to sample the ergodic distribution, we also assume that N is sufficiently large such that the collected $N + K$ samples faithfully capture the statistics of the ergodic measure,

i.e., the stationary solution ρ_* of Eq. (3) satisfying

$$0 = \sum_{i=1}^N \partial_{\phi_i} [\mathbf{R}_i(\phi) \rho_*(\phi)]. \quad (4)$$

In both cases, we assume that each of the observables, g_i , is an L^1 -measurable function against the chosen measure. That is, $\int_{\mathbb{R}^D} \rho(\phi, t) |g_i(\phi)| d\phi < \infty$ for $0 \leq t \leq (K-1)\Delta$ if one chooses a time-dependent distribution in Eq. (3), or $\int_{\mathbb{R}^D} \rho_*(\phi) |g_i(\phi)| d\phi < \infty$ if one chooses a stationary distribution in Eq. 4. We assume that the discrete-time snapshot data \mathbf{D} has sufficiently many samples which capture the statistics of the chosen distribution.

The projection operator. The goal of model coarse-graining is to derive evolutionary equations for the M chosen observables. However, in general, the equations of these observables could depend on under-resolved information that cannot be expressed in terms of the observables themselves. This is the closure problem. To make progress, one must solve the closure problem, to express the evolutionary equation of the observables only in terms of themselves. Mori–Zwanzig formalism leverages on a key construct, the projection operator, to solve the closure problem. Mathematically, consider a real-value function of the full-state $f : \mathbb{R}^D \rightarrow \mathbb{R}$. A projection operator \mathcal{P} is an operator mapping f to another real-value function $(\mathcal{P}f) : \mathbb{R}^M \rightarrow \mathbb{R}$ whose domain is the values of the resolved observables. As such, for any full-state ϕ , after the projection operator, the function is approximated by $(\mathcal{P}f)(g_1(\phi), \dots, g_M(\phi))$. Note that $(\mathcal{P}f)$ can still be expressed a function of the full state ϕ , except that it does not explicitly depend on the under-resolved information. A projection operator \mathcal{P} must satisfies the property $\mathcal{P}^2 = \mathcal{P}$, so that for any f , $\mathcal{P}^n f = \mathcal{P}f$, $n \in \mathbb{N}$. Such a property is critical in derivation of the Mori–Zwanzig formalism [23].

Discrete-time Mori–Zwanzig formalism. Denote the vectorized observable $\mathbf{g} := [g_1, g_2, \dots, g_M]^T$. Following the derivations in [24, 21, 9, 10], the discrete-time Mori–Zwanzig formalism prescribes the exact evolutionary equations of the observables:

$$\mathbf{g}_{n+1}(\phi_0) = \mathbf{\Omega}^{(0)}(\mathbf{g}_n(\phi_0)) + \sum_{\ell=1}^n \mathbf{\Omega}^{(\ell)}(\mathbf{g}_{n-\ell}(\phi_0)) + \mathbf{W}_n(\phi_0). \quad (5)$$

Here, \mathbf{g}_n is an $M \times 1$ vector function of the initial state ϕ_0 such that

$$\mathbf{g}_n(\phi_0) \triangleq \mathbf{g}(\phi(n; \phi_0)) \equiv \mathbf{g}(\mathbf{F}^n(\phi_0)), \quad (6)$$

noting that $\mathbf{g}_0 \equiv \mathbf{g}$. In other words, denote the finite-time (Δ) Koopman operator [25] by \mathcal{K} , $\mathbf{g}_n := \mathcal{K}^n \mathbf{g}$. For clarity, we will write each component of this vector function as $\mathbf{g}_{n,i} := \mathcal{K}^n g_i$. Equation (5), referred to as the Generalized Langevin Equation (GLE), is the central result of the Mori–Zwanzig formalism. It states that \mathbf{g}_{n+1} can be decomposed into three parts: (1) a Markov term of an operator $\mathbf{\Omega}^{(0)} : \mathbb{R}^M \rightarrow \mathbb{R}^M$, mapping an observation to an $M \times 1$ vector, (2) a series of memory-dependent term of a series of operators $\mathbf{\Omega}^{(\ell)} : \mathbb{R}^M \rightarrow \mathbb{R}^M$, $\ell = 1, 2, \dots$, mapping past observations to $M \times 1$ vectors, and (3) a series of orthogonal dynamics that consist of operators $\mathbf{W}_n : \mathbb{R}^D \rightarrow \mathbb{R}^M$, $n = 0, 1, \dots$, mapping any initial state ϕ_0 to an $M \times 1$ vector. Interested reader can find a detailed discussion and physical interpretation of the GLE (5) in [9].

Importantly, these operators depend on the choice of the projection operator \mathcal{P} [24, 21]:

$$\Omega^{(n)} := \mathcal{P}\mathcal{K}[(1 - \mathcal{P})\mathcal{K}]^n, \quad (7)$$

$$\mathbf{W}_n := [(1 - \mathcal{P})\mathcal{K}]^{n+1} \mathbf{g}, \quad (8)$$

with $n \in \mathbb{Z}_{\geq 0}$. Because $\mathcal{P}\mathbf{W}_n = 0$, \mathbf{W}_n is often referred to as the orthogonal dynamics. Below, we will denote the function composition by the symbol \circ . For any initial condition $\phi_0 \in \mathbb{R}^D$ and any $\ell \geq 1$, applying $\Omega^{(\ell)}$ defined in Eq. (7) to $\mathbf{g}_{n-\ell}(\phi_0)$:

$$\begin{aligned} \Omega^{(\ell)} \circ \mathbf{g}_{n-\ell}(\phi_0) &= \mathcal{P}\mathcal{K}[(1 - \mathcal{P})\mathcal{K}]^\ell \mathbf{g} \circ \mathbf{F}^{n-\ell}(\phi_0) \\ &= \mathcal{P}\mathcal{K}\mathbf{W}_{\ell-1} \circ \mathbf{F}^{n-\ell}(\phi_0) \\ &= \mathcal{P}\mathbf{W}_{\ell-1} \circ \mathbf{F}^{n-\ell+1}(\phi_0) \\ &= \mathcal{P}(\mathbf{W}_{\ell-1} \circ \mathbf{F} \circ \mathbf{g}_{n-\ell})(\phi_0). \end{aligned} \quad (9)$$

We used Eq. (6) to established the first equality, and Eq. (8) for the second equality. The third equality follows from definition of the discrete-time Koopman operator \mathcal{K} , that for any function f of ϕ_0 , $\mathcal{K}f = f \circ \mathbf{F}(\phi_0)$. Because Eq. (9) is general for any ϕ_0 , we can equate the following operator identity

$$\Omega^{(\ell)} = \mathcal{P}(\mathbf{W}_{\ell-1} \circ \mathbf{F}), \forall \ell \in \mathbb{Z}_{\geq 0}. \quad (10)$$

The relationship between the memory operators $\Omega^{(\ell)}$ and the orthogonal dynamics $\mathbf{W}_{\ell-1}$ is referred to as the *generalized fluctuation-dissipation relation* (GFD). Below, we will show that how one can use this relationship for data-driven learning.

Regression. Here, we provide a short description of the parametric regression analysis. In regression analysis, the goal is to identify a model f as a function of the independent variables \mathbf{x} for predicting the dependent variables \mathbf{y} . We first focus on one univariate dependent variable y , which can be one of the many components of a vector \mathbf{y} . In parametric regression, the model f is defined as a family of functions $f(\mathbf{x}; \boldsymbol{\theta})$ of the independent variables \mathbf{x} , parametrized by an array of parameters $\boldsymbol{\theta}$. The assumption of the (homoscedastic) regression model is that, in the most general form, there exists a random variable ε such that the random dependent variable y can be expressed as

$$Y(\mathbf{x}) = f(\mathbf{x}; \boldsymbol{\theta}_*) + \varepsilon. \quad (11)$$

The best-fit parameters $\boldsymbol{\theta}_*$ minimizes the error between the model prediction $f(\mathbf{x}; \boldsymbol{\theta})$ and the dependent variable y , given a list of realized samples $\{\mathbf{x}^{[i]}, y^{[i]}\}_{i=1}^N$. The best-fit parameter $\boldsymbol{\theta}_*$ is solved by minimizing a negative log-likelihood function that depends on the noise distribution. For example, for normally distributed ε , the negative log-likelihood function is proportional to the mean squared error (MSE), so one can find the best-fit parameter as the minimizer

$$\boldsymbol{\theta}_* := \arg \min_{\boldsymbol{\theta}} \frac{1}{N} \sum_{i=1}^N (y^{[i]} - f(\mathbf{x}^{[i]}; \boldsymbol{\theta}))^2. \quad (12)$$

Throughout the rest of the manuscript, we will use the mean squared error (MSE) function

as the cost function for the minimization problem. When the dependent variables are multivariate, say \mathbf{y} is $M > 1$ dimensional, we will assume the cost function is the sum of the MSE of M -independent regression models:

$$\boldsymbol{\theta}_* := \arg \min_{\boldsymbol{\theta}} \frac{1}{N} \sum_{i=1}^N \sum_{j=1}^M \left(y_j^{[i]} - f_j(\mathbf{x}^{[i]}; \boldsymbol{\theta}) \right)^2. \quad (13)$$

We remark that our choice comes with three assumptions in the noise model: First, in each component j of the M -dimensional \mathbf{y} , the noise ε_j is normally distributed. Second, the noise ε_j are independently and identically distributed in each of the dimension. Third, the noise is homoscedastic, which means that it does not depend on the independent variable \mathbf{x} . We remark that the negative log-likelihood function can take a different form if one chooses a different noise model (e.g., correlated or heteroscedastic noise). Nevertheless, our results below is general. As such, we will express a general cost function by

$$C\left(\boldsymbol{\theta}; \{\mathbf{x}^{[i]}, \mathbf{y}^{[i]}\}_{i=1}^N\right), \quad (14)$$

so the best-fit parameters $\boldsymbol{\theta}_*$ are solved by the following minimization problem:

$$\boldsymbol{\theta}_* := \arg \max_{\boldsymbol{\theta}} C\left(\boldsymbol{\theta}; \{\mathbf{x}^{[i]}, \mathbf{y}^{[i]}\}_{i=1}^N\right). \quad (15)$$

Regression-based projection operators. We now introduce the regression-based projection operators. Using the notations defined above, we will treat any multivariate function $\mathbf{h} : \mathbb{R}^D \rightarrow \mathbb{R}^M$ of the full-space state $\boldsymbol{\phi} \in \mathbb{R}^D$ as the dependent variable, and the set of observables $\mathbf{g}(\boldsymbol{\phi})$ as the independent variables. We assume that both the dependent and the independent variables are generated from the same full-system configuration $\boldsymbol{\phi}^{[i]}$, which is never accessed, indexed by i and drawn from the induced distribution in our designed simulation. We regress $h(\boldsymbol{\phi})$ on the observed values $\mathbf{g}(\boldsymbol{\phi})$ using a family of multivariate functions $\mathbf{f}(\mathbf{g}(\boldsymbol{\phi}); \boldsymbol{\theta})$ by minimizing a designed cost function:

$$\boldsymbol{\theta}_* := \arg \max_{\boldsymbol{\theta}} C\left(\boldsymbol{\theta}; \left\{\mathbf{g}\left(\boldsymbol{\phi}^{[i]}\right), \mathbf{h}\left(\boldsymbol{\phi}^{[i]}\right)\right\}_{i=1}^N\right). \quad (16)$$

The best-fit $\mathbf{f}(\cdot; \boldsymbol{\theta}_*) : \mathbb{R}^M \rightarrow \mathbb{R}^M$ is now a function that depends on only the observables \mathbf{g} only. It is clear that if we regress $\mathbf{f}(\cdot; \boldsymbol{\theta}_*)$ again on the independent variables $\mathbf{g}(\boldsymbol{\phi})$, we obtain $\mathbf{f}(\cdot; \boldsymbol{\theta}_*)$ again. As such, we can identify the regression analysis is a projection mapping h to $f(\cdot; \boldsymbol{\theta}_*)$:

$$\mathcal{P}\mathbf{h} = \mathbf{f}(\cdot; \boldsymbol{\theta}_*). \quad (17)$$

In summary, with the choice of using regression for projection, applying \mathcal{P} to any function \mathbf{h} of the full-system state $\boldsymbol{\phi}$ results in the best-fit parametric function $\mathbf{f}(\cdot; \boldsymbol{\theta}_*)$ of the reduced-order observables \mathbf{g} .

Learning regression-based Mori–Zwanzig operators by snapshot data. We now use the snapshot data matrix \mathbf{D} to learn the Mori–Zwanzig memory kernels $\boldsymbol{\Omega}^\ell$ and orthogonal

dynamics \mathbf{W}_n , $\ell = 0 \dots$. Setting $n = 0$, the GLE (5) with the expression Eq. (7) states

$$\begin{aligned} \mathbf{g}_1(\phi_0) &\equiv (\mathbf{g} \circ \mathbf{F})(\phi_0) = \mathcal{PK}(\mathbf{g}_0(\phi_0)) + \mathbf{W}_0(\phi_0) \\ &= \mathcal{P}[(\mathbf{g} \circ \mathbf{F})(\phi_0)] + \mathbf{W}_0(\phi_0). \end{aligned} \quad (18)$$

for any given initial condition ϕ_0 . Again, we used the definition of the Koopman operator $\mathcal{K}(\mathbf{g}_0(\phi_0)) = (\mathbf{g}_0 \circ \mathbf{F})(\phi_0)$, which are the observations made at one time step ahead of the initial condition ϕ_0 , and these observations can be accessed in snapshot data \mathbf{D} : they are simply $\mathbf{D}(\cdot, \cdot, 2)$. Note also that $\mathbf{g}(\phi_0)$ can be assessed in snapshot data \mathbf{D} as well—they are $\mathbf{D}(\cdot, \cdot, 1)$. The regression-based \mathcal{P} now projects the function $(\mathbf{g} \circ \mathbf{F})(\phi_0)$ to a function of $\mathbf{g}(\phi_0)$ through regressing $\mathbf{D}(\cdot, \cdot, 2)$ on $\mathbf{D}(\cdot, \cdot, 1)$. For example, using the MSE cost function (13), we solve the following optimization problem for projection:

$$C^{(0)}(\boldsymbol{\theta}; \mathbf{D}) := \frac{1}{N} \sum_{i=1}^N \sum_{j=1}^M \left[\mathbf{D}(i, j, 2) - \mathbf{f}_j \left(\{\mathbf{D}(i, k, 1)\}_{k=1}^M; \boldsymbol{\theta} \right) \right]^2, \quad (19a)$$

$$\boldsymbol{\theta}_*^{(0)} := \arg \min_{\boldsymbol{\theta}} C^{(0)}(\boldsymbol{\theta}; \mathbf{D}), \quad (19b)$$

$$\boldsymbol{\Omega}^{(0)} = \mathcal{P}(\mathbf{g} \circ \mathbf{F}) \equiv \mathbf{f}(\cdot; \boldsymbol{\theta}_*^{(0)}), \quad (19c)$$

where $\mathbf{f}(\cdot; \boldsymbol{\theta}) : \mathbb{R}^M \rightarrow \mathbb{R}^M$ is a family of regressional function. Next, immediately from Eq. (18), we identify the orthogonal dynamics \mathbf{W}_0 is the *residual* of the regression problem:

$$\mathbf{W}_0 = (\mathbf{g} \circ \mathbf{F})(\phi_0) - \mathbf{f} \left(\{\mathbf{D}(k, 0, i)\}_{k=1}^M; \boldsymbol{\theta}_*^{(0)} \right), \quad (20)$$

whose j^{th} component of i^{th} sample can be computed from the snapshot data \mathbf{D} :

$$(\mathbf{W}_0)_j^{(i)} = \mathbf{D}(j, 1, i) - \mathbf{f}_j \left(\{\mathbf{D}(k, 1, i)\}_{k=1}^M; \boldsymbol{\theta}_*^{(0)} \right). \quad (21)$$

As such, we established that $\boldsymbol{\Omega}^{(0)} \equiv \mathcal{P}(\mathbf{g} \circ \mathbf{F})$ and samples of \mathbf{W}_0 can be extracted from the snapshot data set \mathbf{D} .

We now use mathematical induction to show that we can extract $\boldsymbol{\Omega}^{(n+1)}$ and samples of \mathbf{W}_{n+1} , given $\boldsymbol{\Omega}^{(k)}$, $k = 0 \dots n$, using the snapshot data \mathbf{D} . We first use GLE (5) to express the operator \mathbf{W}_n in terms of $\boldsymbol{\Omega}^k$'s:

$$\mathbf{W}_n = \mathbf{g}_{n+1} - \sum_{\ell=0}^n \boldsymbol{\Omega}^{(\ell)} \circ \mathbf{g}_{n-\ell} = \mathbf{g} \circ \mathbf{F}^{n+1} - \sum_{\ell=0}^n \boldsymbol{\Omega}^{(\ell)} \circ \mathbf{g} \circ \mathbf{F}^{n-\ell} \quad (22)$$

Then, we use the GFD, Eq. (10) to construct $\Omega^{(n+1)}$:

$$\begin{aligned}\Omega^{(n+1)} &= \mathcal{P} \left[\left(\mathbf{g} \circ \mathbf{F}^{n+1} - \sum_{\ell=0}^n \Omega^{(\ell)} \circ \mathbf{g} \circ \mathbf{F}^{n-\ell} \right) \circ \mathbf{F} \right] \\ &= \mathcal{P} \left(\mathbf{g} \circ \mathbf{F}^{n+2} - \sum_{\ell=0}^n \Omega^{(\ell)} \circ \mathbf{g} \circ \mathbf{F}^{n-\ell+1} \right).\end{aligned}\quad (23)$$

We recognize that $\mathbf{g} \circ \mathbf{F}^k$ is the observations made at the k^{th} step (including the initial condition), i.e., $\mathbf{D}(\cdot, k+1, \cdot)$, and $\Omega^{(\ell)}$ can be expressed as the best-fit parametric function in the ℓ^{th} optimization problem, $\mathbf{f}(\cdot; \boldsymbol{\theta}_*^{[\ell]})$. Recall that the projection operator \mathcal{P} is operationally an optimization problem, similar to Eq. (24):

$$\mathbf{y}_{i,j}^{(n+1)} := \mathbf{D}(i, j, n+3) - \sum_{\ell=0}^n \mathbf{f}_j \left(\{\mathbf{D}(i, k, n-\ell+2)\}_{k=1}^M; \boldsymbol{\theta}_*^{(\ell)} \right), \quad (24a)$$

$$C^{(n+1)}(\boldsymbol{\theta}; \mathbf{D}) := \frac{1}{N} \sum_{i=1}^N \sum_{j=1}^M \left[\mathbf{y}_{i,j}^{(n+1)} - \mathbf{f}_j \left(\{\mathbf{D}(i, k, 1)\}_{k=1}^M; \boldsymbol{\theta} \right) \right]^2, \quad (24b)$$

$$\boldsymbol{\theta}_*^{(n+1)} := \arg \min_{\boldsymbol{\theta}} C^{(n+1)}(\boldsymbol{\theta}; \mathbf{D}), \quad (24c)$$

$$\Omega^{(n+1)} \equiv \mathbf{f}(\cdot; \boldsymbol{\theta}_*^{(n+1)}). \quad (24d)$$

Thus by induction, we can iteratively extract $\Omega^{(n)}$, $n = 0 \dots N-2$ (in total, $N-1$ ones), using the collected snapshot data \mathbf{D} .

We remark that both the orthogonality $\mathcal{P}\mathbf{W}_n = 0$ and the Generalized Fluctuation-Dissipation relation, $\Omega^{(n+1)} = \mathcal{P}\mathcal{K}\mathbf{W}_n$ are built in by construction.

A special case: linear regression. We now show that selecting the a special choice of regression, the multivariate linear regression, results in the discrete-time algorithm we proposed in [9]. Linear regression postulates that the parametric form of \mathbf{f} :

$$\mathbf{f}(\mathbf{g}) := \boldsymbol{\beta} \cdot \mathbf{g}, \quad (25)$$

in which we assume the feature vector \mathbf{g} contains a constant 1, which accounts for the biased term in linear regression analysis. Here, the parameters $\boldsymbol{\theta}$ is the list of entries of $M \times M$ matrix $\boldsymbol{\beta}$. The best-fits of linear regression analysis are analytically tractable. Define the $N \times M$ data matrix \mathbf{X} at time $k-1$ whose entries are $\mathbf{X}_{i,j}(k-1) := \mathbf{D}(i, j, k)$. The solution of Eqs. (24) is

$$\Omega_*^{(0)} = (\mathbf{X}^T(1) \cdot \mathbf{X}(0)) \cdot (\mathbf{X}^T(0) \cdot \mathbf{X}(0))^{-1}, \quad (26)$$

which is $\mathbf{C}(1) \cdot \mathbf{C}^{-1}(0)$, where $\mathbf{C}(k) := \mathbf{X}^T(k) \cdot \mathbf{X}(0)$ is the empirical k -lag correlation matrix of the observables induced by the dynamics. Equation (26) is precisely the extracted Markov term in [9], and the approximate Koopman operator [12, 13, 14]. As for the higher orders,

Eq. (24a) can be expressed as

$$\mathbf{y}^{(n+1)} := \mathbf{X}(n+2) - \sum_{\ell=0}^n \boldsymbol{\Omega}_*^{(\ell)} \cdot \mathbf{X}(n-\ell+1), \quad (27)$$

leading to the solution of the minimization problem Eqs. (24b)-(24d):

$$\boldsymbol{\Omega}_*^{(n+1)} = \left[\mathbf{C}(n+2) - \sum_{\ell=0}^n \boldsymbol{\Omega}_*^{(\ell)} \cdot \mathbf{C}(n-\ell+1) \right] \cdot \mathbf{C}^{-1}(0), \quad (28)$$

which is exactly the formula derived from the GLE with Mori's projection operator for computing $\boldsymbol{\Omega}^{(n)}$'s in [9]. Because our analysis in [9] was based on Mori's projection operator [1], it is clear that choosing linear regression as the regression-based projection operator corresponds to Mori's linear projection operator.

Making predictions and modeling orthogonal dynamics. We will focus on the goal of using the GLE (5) to make multi-step prediction for the reduced-order observables \mathbf{g}_k , $k \geq 1$, given a series of the current and the past observables, \mathbf{g}_n , $n = 0, -1 \dots H$. To achieve this, we will repetitively use GLE (5). We first use it to predict \mathbf{g}_1 . Then, we accumulate the predicted \mathbf{g}_1 into the series of observations, \mathbf{g}_n , $n = 0, -1 \dots H$, and use this accumulated series to make prediction of \mathbf{g}_2 using (5) again. The procedure continues until the desired finite horizon $k \geq 1$ is reached. Clearly, the orthogonal dynamics \mathbf{W}_k , $k \geq H$, are needed in the procedure. Recall that the orthogonal dynamics encodes the information that live in the orthogonal space (Eq. (8)), and thus cannot be resolved. Modeling the orthogonal dynamics is challenging: it is equivalent to modeling the effects of all the under-resolved degrees of freedom on the resolved part of the dynamics. The modeling is highly specific to the full dynamics and the choice of the resolved observables.

A best-case scenario is that the resolved observables are reasonably selected, and an expressive enough regression model is chosen. With a sufficiently long history length H , this will lead to negligible orthogonal dynamics, i.e., the residuals of the regression analysis are small enough to be ignored. In below numerical experiments, we will assume we are close to this scenario and proceed with a trivial zero-noise model $\mathbf{W}_n = 0$, $n \geq H$, despite the finite residuals in the experiments.

We also tested the standard way of fitting the residual \mathbf{W}_n as independent and multi-variate Gaussian distribution (independent in the time index n). The predictions are qualitatively similar but more noisy as the predictions are based on realizations of the orthogonal dynamics, now modeled as random variables. As the results are similar but less "clean", we will not present the results with the noise model modeling the residual dynamics in this article.

Nonlinear regression on linear functional basis vs. linear regression on nonlinear functional basis. It is useful to juxtapose the nonlinear regression-based projection operator with the Mori's projector, which is a linear Koopman representation with nonlinear functional basis [1, 14, 9]. Although Koopman representation is linear—potentially with nonlinear functional basis [14]—with the benefit that the learning is a simple convex problem, it comes with two shortcomings.

First, the prediction in the Koopman representation is always linear in the observables. The linearity exclude closure schemes with nonlinear relationship, and thus, Koopman representation and equivalently Mori's projection operator are not compatible with many nonlinear closure methods developed in model coarse-graining. In contrast, a nonlinear regression-based projection operator is suitable for nonlinear closure scheme.

To illustrate this problem, let us consider a hypothetical, one-dimensional nonlinear dynamical system whose state is $\phi \in \mathbb{R}^1$. Suppose we choose three lowest-order polynomial functions as the nonlinear basis function, so the observables are defined by $\mathbf{g} \circ \phi = [\phi^0, \phi^1, \phi^2]^T$. Assuming that these polynomial functions do not span a Koopman invariant space. Now, supposed we performed the data-driven learning for the Mori-Zwanzig operators $\Omega^{(\ell)}$, $\forall \ell$, using the snapshot data and algorithms presented in [9]. With Mori's projection, the MZ operators $\Omega^{(\ell)}$ are 3×3 matrices. Next, suppose we wish to use the learned operators and the GLE (5) to make predictions for the reduced-order observables, provided a series of present and past snapshots of $\mathbf{g}_0, \mathbf{g}_{-1}, \dots, \mathbf{g}_{-H}$ with some history length $H \geq 0$. Clearly, each component of the predicted \mathbf{g}_1 by GLE (5) is a linear sum of the components of \mathbf{g}_n , $n = 0 \dots -H$, and \mathbf{W}_H . Similarly, each component of \mathbf{g}_2 by GLE (5) is a linear sum of the the components of \mathbf{g}_n , $n = 0 \dots -H$, \mathbf{W}_H , and \mathbf{W}_{H+1} . Note that the dependence on \mathbf{g}_1 can be suppressed and rewritten as a linear sum of the components \mathbf{g}_n , $n = 0 \dots -H$ and \mathbf{W}_H . In general, any prediction \mathbf{g}_k , $k \geq 1$ is linear in the components of $\mathbf{g}_n = 0 \dots -H$ and those of \mathbf{W}_m , $m = H \dots H + k - 1$. A special case of $H = 0$ converges to the prediction made by only the approximate Koopman operator. In any case, the predictions based on Mori's projection operator are always *linear combination of the given observables*. This is inconsistent with nonlinear closure scheme, where the reduced-order models can have terms that are nonlinear in the observables.

A relevant pitfall of Mori's projection operator is the above predictions cannot satisfy the trivial nonlinear relationship $g_{n,2} = g_{n,1}^2$, $\forall n \geq 0$, established from the definition of the Koopman operator, that for any initial condition ϕ_0 :

$$\begin{aligned} g_{n,2} \circ \phi_0 &= (\mathcal{K}_{\Delta}^n g_2)(\phi_0) = g_2 \circ (\phi(n\Delta; \phi_0)) = \phi^2(n\Delta; \phi_0) \\ &= [g_1 \circ (\phi(n\Delta; \phi_0))]^2 = [(\mathcal{K}_{\Delta}^n g_1)(\phi_0)]^2 = (\mathcal{K}_{\Delta}^n g_1)^2(\phi_0) = g_{n,1}^2 \circ \phi_0. \end{aligned} \quad (29)$$

We remind the reader that we used $g_{n,m}$ to denote the n th step prediction of the m th observable. The inconsistency in approximate Koopman or Mori's projection operator is came from the choice that one always expresses $g_{n,2}$, $n \geq 1$, in terms of linear combination of $g_{0,0}$, $g_{0,1}$, and $g_{0,2}$. In below numerical numerical experiments, we will see how the perdition with this projection operator can lead to extremely unsatisfactory results.

On the contrary, suppose we go with a nonlinear polynomial regression on a single observable $g_{0,1}$ with a comparable nonlinearity, $\Omega^{(\ell)}(g_{0,1}) = \alpha^{(\ell)} + \beta^{(\ell)}g_{0,1} + \gamma^{(\ell)}g_{0,1}^2$, where the parameters $\theta^{(\ell)}$ of the regression model are three real-valued numbers $(\alpha^{(\ell)}, \beta^{(\ell)}, \gamma^{(\ell)})$. Suppose we carried out the nonlinear regression-based regressions and obtained the optimal $\theta_*^{(\ell)}$, $\forall \ell \geq 0$. We next use the learned parameters to make prediction, provided a series of present and past snapshots of $\mathbf{g}_0, \mathbf{g}_{-1}, \dots, \mathbf{g}_{-H+1}$. With the GLE (5) and the nonlinear-regression

projection operator, the first-step prediction is

$$g_{1,1} = \left(\sum_{\ell=0}^H \alpha_*^{(\ell)} + \beta_*^{(\ell)} g_{-\ell,1} + \gamma_*^{(\ell)} g_{-\ell,1}^2 \right) + W_H, \quad (30)$$

which is identical to the prediction of Mori’s projection operator with the three lowest polynomial functions. However, in the second step, the GLE would induce nonlinearity in the components of $g_{1,1}^2$:

$$\begin{aligned} g_{2,1} &= \left(\sum_{\ell=0}^{H+1} \alpha_*^{(\ell)} + \beta_*^{(\ell)} g_{1-\ell,1} + \gamma_*^{(\ell)} g_{1-\ell,1}^2 \right) + W_{H+1}, \\ &= \alpha_*^{(0)} + \beta_*^{(0)} g_{1,1} + \gamma_*^{(0)} g_{1,1}^2 + \left(\sum_{\ell=1}^{H+1} \alpha_*^{(\ell)} + \beta_*^{(\ell)} g_{1-\ell,1} + \gamma_*^{(\ell)} g_{1-\ell,1}^2 \right) + \mathbf{W}_{H+1}. \end{aligned} \quad (31)$$

Clearly, the term $g_{1,1}^2$ in the above equation introduces higher-order nonlinear functions of the observables in the present and past snapshots, $\mathbf{g}_{n,1}$, $n = 0 \dots -H$. Such a nonlinear predictive model is consistent with the nonlinear closure schemes, that *the coarse-grained model is again a nonlinear dynamical system of the reduced-order variables*.

The second shortcoming of the approximate Koopman’s computation is that its functional bases— g_i ’s in the above example—have to be specified *a priori*. There exist methods that use NNs for learning the functional basis [18, 19, 20]. These methods advocate the idea of using NNs for learning optimal nonlinear basis functions for data-driven Koopman learning [14]. However, NNs are generally nonlinear functions of the input features, so the joint learning problem (i.e., learning the functional basis and the approximate Koopman operator) loses the benefit of linearity and global convexity. In addition, NNs are prone to over-fitting, so a heuristic regularization has to be imposed, leading to a different optimization problem from the original approximate Koopman [14] or Mori’s [9] setup. As a consequence, it is difficult to generalize data-driven learning with Mori’s projection operator [1, 9] (or equivalently the ortho-normalized finite-rank projection operator [3]) for these existing data-driven learning methods for dynamical systems. In contrast, regression-based projection operators bypass the linearity constraint. Our theoretical construct can thus (1) accommodate nonlinear basis function optimization by simply formulating $\mathbf{f}(\mathbf{x}; \boldsymbol{\theta}) = \sum_{i=1}^M \mathbf{K} \cdot \mathbf{f}_i(\mathbf{x}; \boldsymbol{\theta})$ where \mathbf{f}_i ’s are the unknown basis functions to be constrained by data, and the linear map \mathbf{K} is based on the postulation that the final function is a linear combination of the (unknown) basis function, and (2) accommodate regularization by simply formulating a general cost function (Eq. (14)) with a regularization term. As such, we viewed the regression-based Mori–Zwanzig formalism as the most natural and accurate mathematical construct for heuristic DNN-based learning methods [18, 19, 20].

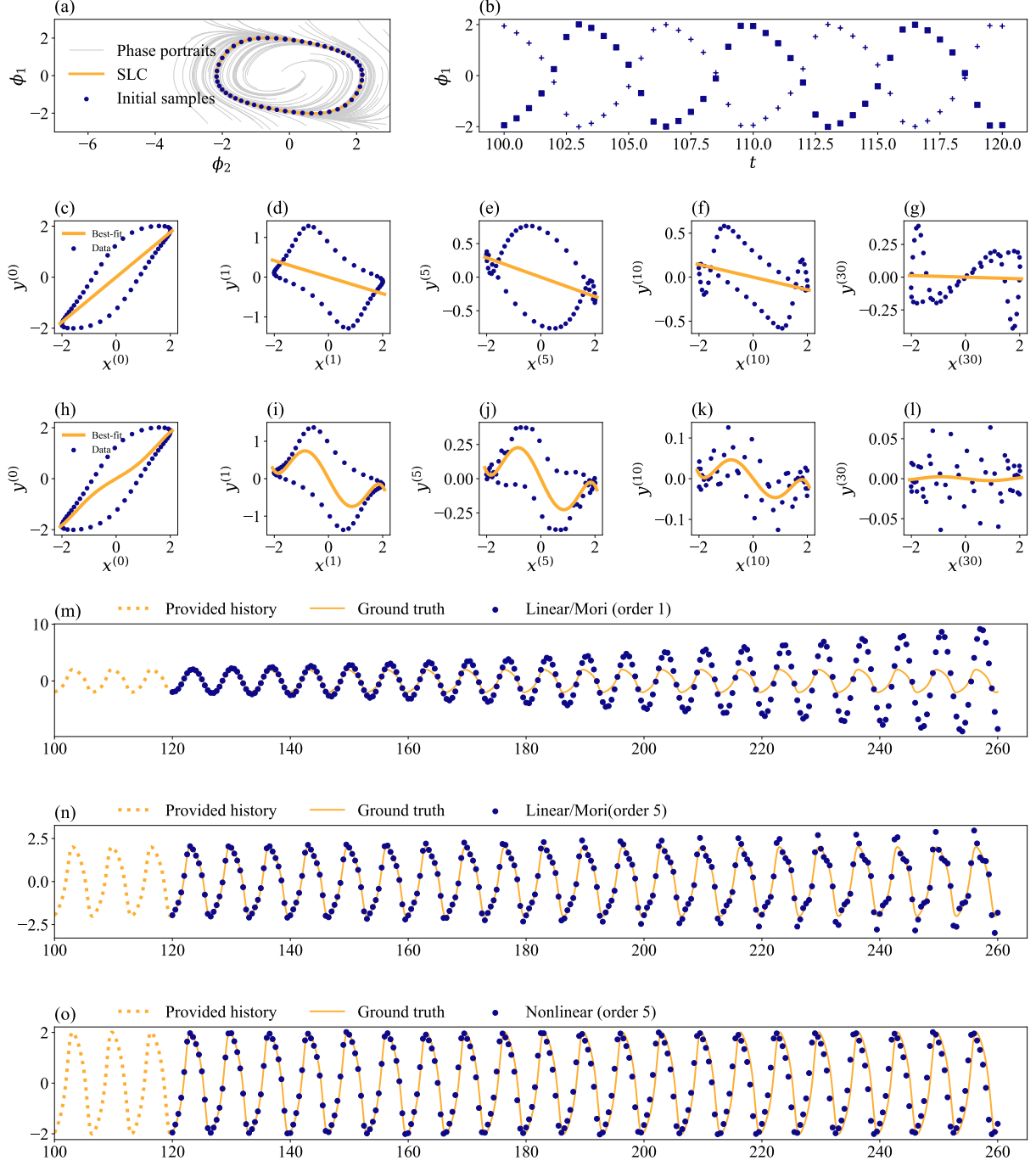


Figure 1: The Van der Pol oscillator. (a) The phase portraits of the full system, the stable limit cycle (SLC), and the initial samples of the data matrix $\mathbf{D}(\cdot, 1, 1)$; (b) Snapshot samples along two trajectories, $\mathbf{D}(1, 1, \cdot)$ and $\mathbf{D}(26, 1, \cdot)$; (c-g) Linear regression with a single observable, $f_\theta(x) := \theta x$; (h-l) Nonlinear polynomial regression with a single observable, $f_\theta := \sum_{i=0}^5 \theta_i x^i$; (m-o) Prediction of the learned (m) linear regression with polynomial basis function up to order 1, g_0 and g_1 , $g_i(x) \triangleq x^i$, (n) linear regression with polynomial basis function up to order 5, g_i , $i = 0, \dots, 5$, $g_i(x) \triangleq x^i$, and (o) nonlinear polynomial regression up to order 5.

2.2 Numerical Analysis

2.2.1 An illustrative example: the Van der Pol oscillator

We used the Van der Pol oscillator as an example to illustrate the regression-based Mori–Zwanzig formalism.

The Van der Pol oscillator is a two-dimensional nonlinear system, which follows

$$\frac{d}{dt}\phi_1(t) = \mu \left(\phi_1 - \frac{\phi_1^3}{3} \right) - \phi_2, \quad (32a)$$

$$\frac{d}{dt}\phi_2(t) = \frac{1}{\mu}\phi_1. \quad (32b)$$

We chose $\mu = 1$ in this illustrative example. The Van der Pol oscillator has a global limit cycle, which is a one-dimensional manifold embedded in the (ϕ_1, ϕ_2) -state space, as shown in Fig. 1(a). For illustrative purpose, we considered a single observable $g(\phi_1, \phi_2) = \phi_1$, as the resolved dynamic variable. We used `scipy.integrate.solve_ivp` with the `lsoda` method to numerically solve the system from an arbitrarily chosen state $(0, 1)$ and $t_c = 100$ for the system to relax to the limit cycle, whose period is roughly 6.663. We chose 50 initial conditions evenly sampled over one period; these initial conditions are also visualized in Fig. 1(a). Then, we collected snapshot data set \mathbf{D} by measuring $\phi_1(t)$ from $t = 0$ to $t = 20$ every $\Delta = 0.5$ from each of the initial conditions; two of the trajectories as shown in Fig. 1(b). In Figure 15(c)-(g), we show how the Mori’s projection operator [9] is applied to the snapshot data set \mathbf{D} . In Figure 15(c), the $\{x_i^{(0)}, y_i^{(0)}\}_i$ data pairs are simply $\mathbf{D}(i, 1, 1)$ and $\mathbf{D}(i, 1, 2)$. That is, the $x^{(0)}$ ’s are the observed ϕ_1 at the time $t = 0$, and the $y^{(0)}$ ’s are the observed ϕ_1 one step ahead ($t = \Delta$). Because the system is under-resolved, there can be two possible y ’s for most of the measured x on the stable limit cycle (see Fig. 1(a)). Approximate Koopman and Mori’s projector on a single observable is equivalent to a linear regression using $f(x; \theta) = \theta x$ to fit the data. The best-fit line is the projected model, $\theta_*^{(0)} x$. The slope of the best-fit model, $\theta_*^{(0)}$, is the approximate Koopman operator [12, 13, 14] and equivalently the Markov transition matrix in the context of data-driven Mori–Zwanzig formalism [9]. After the first regression is made, the learned model $\theta_*^{(0)}$ is used to predict the system from $t = \Delta$ to 2Δ , $\phi_1^{\text{pred}} = \theta_*^{(0)} \phi_1(\Delta)$. The residual $\phi(2\Delta) - \phi_1^{\text{pred}}$ is assigned to $y_i^{(1)}$. The next linear regression on $\phi_1(0)$ is performed (Fig. 1(d), and the slope of the best-fit line is the first discrete-time memory kernel [9]. The process repeats, and in Figs. 1(e-g), we showed the 5th, 10th, and the 30th linear regression. In Figs (h-l), we used polynomial regression up to degree 5 instead, showing that with same iteration. As expected, the more expressive polynomial regression leads to smaller errors than that of the linear regression.

When there are more than one observables, we used the multivariate linear regression for each of the component of the \mathbf{y} vector, with a set of independent variables that are the components of \mathbf{x} . Multivariate linear regression is functionally identical to the DMD and EDMD.

Figures (m-o) shows the predictions of the learned models. First, we simulated the full system (32) from a different initial condition $(\phi_1, \phi_2) = (1, 0)$ until $t = t_c = 100$ for relaxing the system to the stable limit cycle. Then, we measure ϕ_1 every $\Delta = 0.5$ time until $t = 260$ as

the ground truth of the dynamics. We considered three learned models, including (1) Mori’s projection down to the linear order of ϕ_1 (i.e., two polynomial basis functions g_0 and g_1 , $g_i(\phi_1) \triangleq \phi_1^i$), (2) Mori’s projection down to the first five orders of ϕ_1 (i.e., six polynomial basis functions g_i , $i = 0 \dots 6$, $g_i(\phi_1) \triangleq \phi_1^i$), and (3) a nonlinear regression-based projection operator based on fifth-order polynomial fitting. Given the snapshots in $t \in (100, 120)$, we used the generalized Langevin equation Eq. (5) with $\mathbf{W} := 0$ recursively to predict the dynamics at $t \geq 120$, assuming the orthogonal dynamics \mathbf{W} ’s are small and can be ignored. Figures 1(m) and (n) shows that the error due to the negligence of the orthogonal dynamics accumulates and eventually destabilize the prediction in Mori’s projection formalism. In comparison, Figure 1(o) shows that the nonlinear regression-based projection operator can reasonably approximate the true dynamics for a longer predictive horizon, using only the under-resolved snapshots.

We remark that this example was deliberately constructed as a minimal illustrative example. There is little scientific insights and implications derived from this analysis. After all, there are more suitable methods (e.g., Fourier analysis) for periodic signals. It is our mere intention that, with such a simple system, the visualizations in Fig. 1 can transparently illustrate how the under-resolved degrees of freedom of a deterministic system could induces a distribution and how the data-driven learning based on linear (Mori) and nonlinear regressions is applied to the snapshot data set.

2.2.2 Lorenz ‘63 system

Our second example is the Lorenz (‘63) model [26], which is a three-dimensional system

$$\frac{d}{dt}\phi_1(t) = \sigma(\phi_2 - \phi_1), \quad (33a)$$

$$\frac{d}{dt}\phi_2(t) = \phi_1(\rho - \phi_3) - \phi_2 \quad (33b)$$

$$\frac{d}{dt}\phi_3(t) = \phi_1\phi_2 - \beta\phi_3. \quad (33c)$$

We adopt the original model parameter values which E. Lorenz chose, $(\sigma, \rho, \beta) = (10, 28, 8/3)$. We will consider the “reduced-order model” as the $\phi_1(t)$ alone. A long trajectory with an arbitrarily selected initial condition $(\phi_1, \phi_2, \phi_3) = (0.01, 1, 10)$ was generated using `scipy.integrate.solve_ivp`. We discarded the initial transient before $t = t_c$, and collect 10^6 snapshots of ϕ_1 every $\Delta = 0.01$ until $t = t_c + 10^4$, as the samples on the strange attractor.

We considered five projection operators and compared their performances using the Lorenz ‘63 model, listed by the complexity (expressiveness) of the statistical model below. First, we considered first-order Mori’s projection operator, i.e., the selected basis functions are g_0 and g_1 . We referred to this projection operator, which corresponds to the conventional DMD analysis, as Mori (1). Next, we considered a fifth-order Mori’s projection operator with six polynomial functions, $g_0 \dots g_5$. We referred to this projection operator, which corresponds to an EDMD analysis, as Mori (5). The third projection operator we considered is a nonlinear fifth-order polynomial regression. Next, we considered a projection operator defined by a cubic (degree = 3) spline regression with ten knots (including boundary knots) evenly distributed between 1.5 times of the minimum and maximum samples of the collected ϕ_1

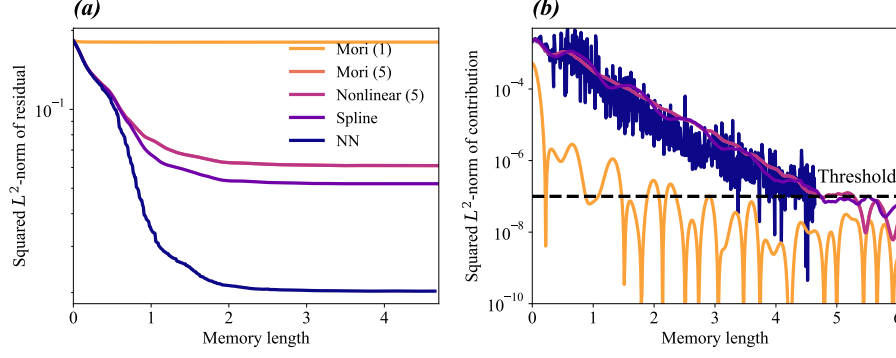


Figure 2: The Lorenz '63 system. (a) The squared L^2 -norm of the validation residual as the memory length increases. (b) The squared L^2 -norm contribution at different memory length. The threshold is set at 10^{-7} for determining the memory length.

samples. After the spline features are generated, we performed a ridge regression with the L^2 regularization parameter set at $\lambda = 10$. Finally, we consider a simple neural network (NN). The architecture of the neural networks is two fully-connected feed-forward layers, each of which contains five artificial neurons, and a third linear layer with only one neuron. We always chose the hyperbolic tangent function as the activation function of the artificial neurons in this manuscript.

We used the measured snapshots to learn the operators $\Omega^{(\ell)}$'s for each of the selected projection operators. Figure 2(a) shows the magnitude of the summary residual, defined as the averaged mean-squared error (MSE) of the ℓ th regression. Recall that ℓ is the index of the memory terms (cf. Eq. (5)). Thus, we plot the summary residual as a function of the physical time of the memory length ($\ell\Delta$) in Fig. 2(a). It is observed that with the increased complexity of the regression model, the residual with memory contribution can decrease significantly, from Mori's projection operator based on only g_0 and g_1 ($\approx 2 \times 10^{-1}$) to the expressive neural network ($\approx 2 \times 10^{-2}$). Note that without the memory contribution ($\ell = 0$), the magnitudes of the summary residual are indistinguishable; the significant improvement comes only with a finite-time memory contribution, ≈ 2.0 . This observation justified the advantage of the Mori-Zwanzig's memory-dependent formulation especially for more expressive models.

To investigate the contribution of the memory effects, we plot the L^2 -norm of the memory contribution in Eq. (5), $\Omega^{(\ell)}(\phi_1(k\Delta))$ averaged over the collected snapshots $k = 1 \dots$. That is, we are choosing each snapshot along the long trajectory as a sample of many initial conditions, and compute the memory contribution ℓ steps into the future. Figure 2(b) shows the memory contribution with various projection operators. We observed that memory contribution generally decays as a function of the memory length, regardless of the chosen regression methods. This observation suggests that a finite length of the memory is sufficient, as the contribution of past history after a certain timescale would be small and negligible. As a result, in the following analysis, we choose a finite memory contribution by thresholding the memory contribution to be greater than 10^{-7} . The corresponding memory lengths are: 236 past snapshots for Mori (1); 470 past snapshots for Mori (5); 470 past snapshots for the nonlinear regression; 470 past snapshots for the spline regression; 470 past snapshots for

neural network.

After the nonlinear memory functions ($\Omega^{(\ell)}$) are learned, we turned our attention to the prediction of the learned models. To make the prediction, a test trajectory was generated from a different initial condition $(\phi_1, \phi_2, \phi_3) = (0, 1, 2)$ discarding the transient $t < t_c = 1000$. We took the past history of the reduced-order variable $\phi_1(1000 \leq t \leq 1050)$ and use Eq. (5) to make predictions for $t > 1050$, assuming (1) the orthogonal dynamics $\mathbf{W} = 0$ and (2) with a finite memory length, i.e., $\Omega^{(\ell)} = 0, \forall \ell \geq \ell_c$, the critical timescale above which the squared L^2 -norm of the memory contribution is less than 10^{-7} . For comparison, we also made prediction from memory-less models, that is, setting $\Omega^{(\ell \geq 1)} = 0$. Note that the memory-less Mori (1) and Mori (5) corresponds to the approximate Koopman models [21].

Figure 3 showed the predictive trajectories from the learned models. For all the methods, we found that the memory-less models failed to capture any characteristics of the under-resolved dynamics, except for its mean in the long time. For Mori (1) and Mori (5), which correspond to higher-order data-driven approximate Koopman models [9], a similar behavior of relaxation to the the mean was observed. This should not be a surprise: as we detailed in our recent work [9], Mori-Zwanzig without the under-resolved orthogonal dynamics is identical to using the two-time correlation functions as the propagators for prediction. As the chaotic system, the two-time correlation function $\langle \phi_1(t), \phi_1(0) \rangle$ decays to 0 because the dynamics de-correlates for a large lag $t \gg 1$. Consequently, Mori (1) and (5) projection operators also made predictions that converge to the mean behavior in the long-time limit. In comparison with the Mori (1), Mori (5) learned a transient oscillation which crudely characterized the short-time dynamics of the Lorenz ‘63 model. We observed that the drawback of the steady long-time behavior is significantly improved when we used nonlinear projection operators. The prediction based on the nonlinear regression showed a much better prediction in a short horizon, and an oscillation between the two wings of the Lorenz butterfly. Notably, the oscillation is not chaotic as it is in the fully resolved system. The prediction based on the spline regression, which is an intermediate model between the nonlinear polynomial regression and the neural-network-based regression models, began to exhibit chaotic behaviors in the long-time limit. Finally, the prediction of the one-dimensional reduced-order model based on the neural network is very similar to the dynamics of the three-dimensional Lorenz ‘63 model, qualitatively speaking. To quantify the performance of the predictions, we first collected the long-time statistics by evolving Eq. (5) for a long time (150,000 steps in total). We plotted the distributions of the collected trajectories based on the learned models in Fig. 4; such empirical distributions would be the stationary distribution if the process is ergodic. Clearly, Mori (1) and (5) showed an almost δ -like distribution at the mean $\langle \phi_1 \rangle = 0$ because their prediction converged to the mean behavior in a finite timescale. All the nonlinear projection operators reasonably approximate the empirical distribution of ϕ_1 which we collected in the solution of the Lorenz ‘63 model. We observed that neural network out-performed the spline regression, which out-performed the plain fifth-order polynomial regression.

We further quantified the predictive error by the following metric. First, we compute the L_2^2 -error of the prediction to the actual dynamics of $\phi_1(t)$. The initial condition and the histories were uniformly sampled along a long trajectory of the actual dynamics. We collected 25,000 samples and compute the mean-squared error as a function of the predictive horizon in Fig. 5(a). As can be seen, models with nonlinear projection operator generally

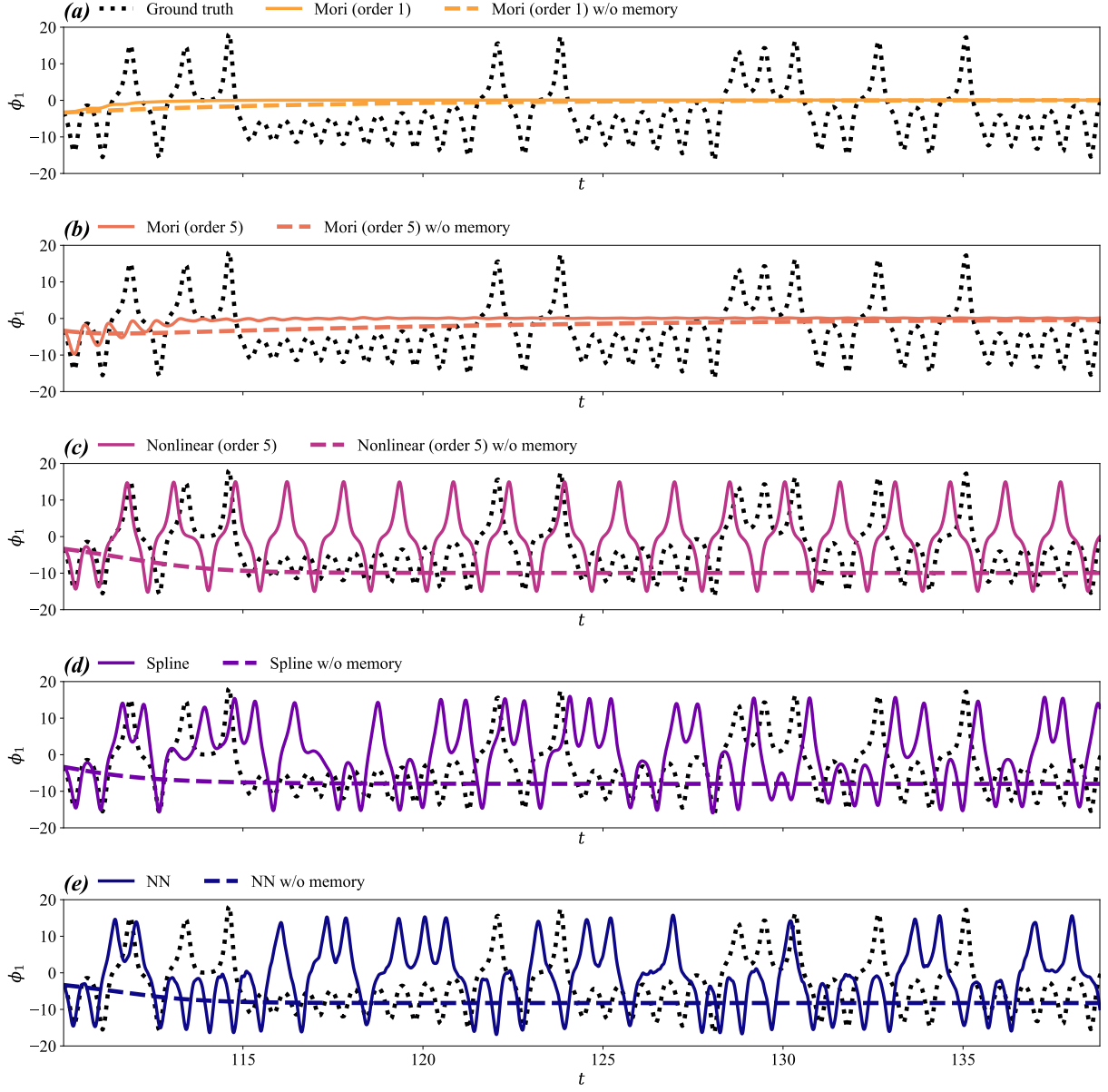


Figure 3: The Lorenz '63 system. (a-e) The predictive trajectories for the learned models based on five different projection operators.

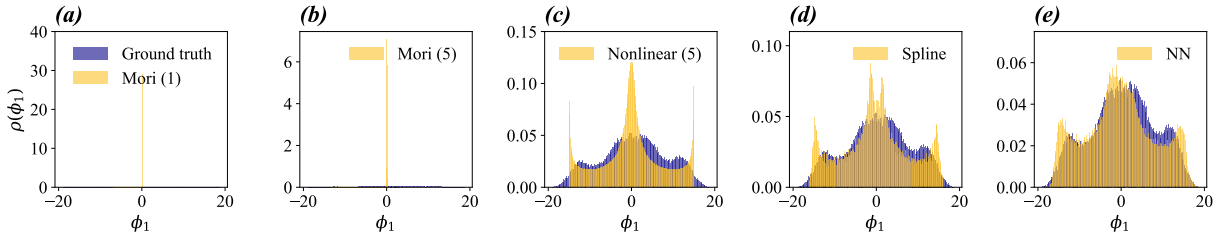


Figure 4: Long-time statistics of the MZ model predictions of the Lorenz '63 model.

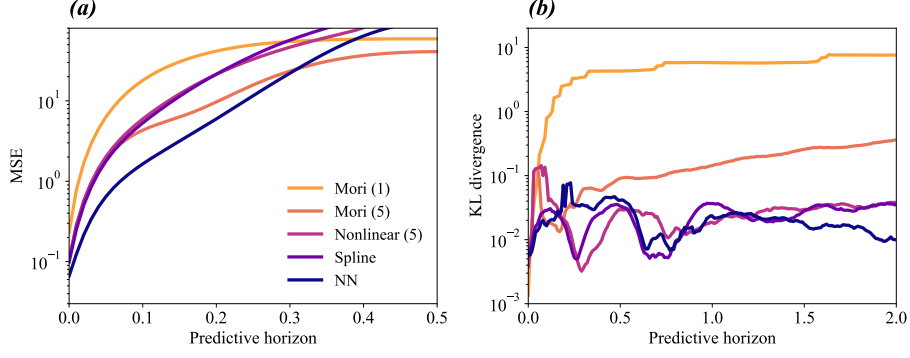


Figure 5: Predictive error of the reduced-order models on the the Lorenz '63 system. (a) The squared L^2 -norm of the prediction error for different predictive horizons; (b) the Kullback–Leibler divergence of the empirical distribution from the model predicted distribution.

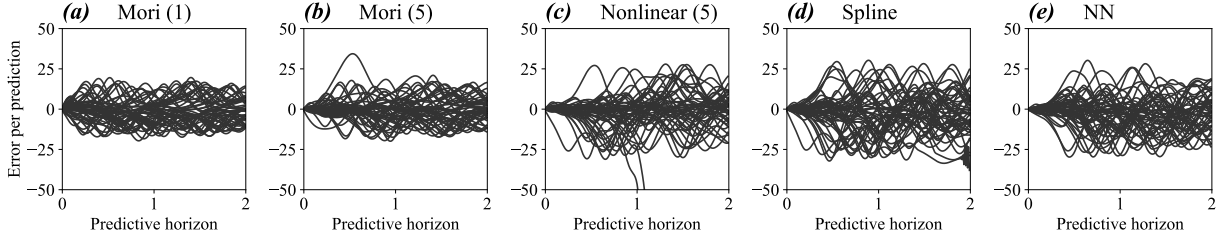


Figure 6: The Lorenz '63 system. (a-e) The deviation of 50 predicted trajectories using the learned models.

predict much better than Mori (1) and (5) do. The errors of the nonlinear models eventually grew larger at a finite predictive horizon ($t \approx 0.3$). We remark that, this should not be considered as a drawback but an advantage: Mori (1) and (5) predict the mean of the chaotic dynamics but nonlinear models would predict similar oscillations in the long run. In terms of the mean squared error, predicting only the mean would have a smaller error but miss out much dynamical features. As such, we also compute the Kullback–Leibler divergence from the predictive distribution (approximated by the histogram of the samples from of the reduced-order models) to the ground truth distribution (approximated by the histogram of the samples from the actual dynamics), as shown in Fig. 5(b). With this metric, we observed that the the reduced-order models based on the nonlinear projection operators captured the time-dependent distribution of ϕ_1 much better than the reduced-order models based on linear projection operators. We conclude this section by discussing the potential pitfalls of nonlinear regression as a projection operator. Mainly, the stability of the learned models is not always guaranteed. We observed that the learned reduced model, given some of the initial condition and histories, can blow up in finite time. In Fig. 6, we plotted the deviation of the prediction from the actual dynamics. For each of the reduced-order models, we plotted 50 deviations, whose initial condition and histories sampled on a long ground-truth trajectory. We observed that for plain nonlinear, fifth-order polynomial regression, the learned model could explode in finite time. The spline regression, which

predicts constants outside of the boundary knots in contrast to polynomial blowup of the nonlinear regression, seemed to alleviate the problem. However, when the prediction goes beyond the data distribution, the spline regression can also be “trapped” locally and induce high-frequency oscillations. Interestingly, we did not observe these pathologies in the neural network.

2.3 Kuramoto–Sivashinsky Equation

Our third example is the Kuramoto–Sivashinsky (KS) equation which was developed in 1970’s for modeling instability of flame propagation [27, 28, 29]. Specifically in this study, we consider the one-dimensional KS (partial differential) equation

$$0 = \frac{\partial}{\partial t} u(x, t) + \frac{\partial^2}{\partial x^2} u(x, t) + \frac{\partial^4}{\partial x^4} u(x, t) + u(x, t) \frac{\partial}{\partial x} u(x, t), \quad (34a)$$

for all time $t \geq 0$ on a bounded domain $x \in [0, L]$, given initial data $u(x, 0) = u_0(x)$. A periodic boundary condition is imposed, $u(t, 0) = u(t, L) \forall t$. In this study, we chose $L = 16\pi$ and uniformly discretized the space into $N = 128$ points. We used the pseudo-spectral forth-order exponential time-derivative Runge–Kutta (ETDRK4) algorithm [30] with 2/3-dealiasing [21] to solve the spatially discretized system. The time step for the explicit ETDRK4 algorithm was set as 10^{-3} , and we observe every 10^3 steps (so $\Delta = 1$). For the training data, we followed [30] and set $u_0^{\text{tr}}(x) = \cos(2\pi x/L) [1 + \sin(2\pi x/L)]$, and for the test data, $u_0^{\text{te}}(x) = \sin(2\pi x/L) [1 + \cos(2\pi x/L)]$. Both the training and the validation sets were simulated to $t = t_c + 10^5$, and we discarded the transient trajectories before $t_c = 5 \times 10^2$.

We considered a four-fold reduced-order model by only observing the variable u every four discretized spatial grids. That is, $\{u(t, x_{4i})\}_i$, where $i = 0, 1, \dots, 31$ is the grid index. We augmented the reduced-order data set by two operations. (1.) *Shifting*: we used samples collected on different sub-grids: $u(t, x_{4i+j})$, $j = 0, 1, 2, 3$ and (2.) *Reordering*: we imposed the C_1 symmetry of the system, i.e., $u(t, x_{\text{mod}(4(i+k)+j, 32)})$, $k = 0, 1, \dots, 31$.

With the KS equation example, we also adopted and integrated the delay-embedding technique into some of the regression-based models. With delay embedding, the input of the regression analysis is augmented to include a finite number (henceforth referred as H) of past snapshots [31, 20]. As remarked in the discussion in our previous study [9], the memory dependence in the delay-embedding technique is not the memory effect in the Mori–Zwanzig formalism. We will provide a more detailed discussion provided in the Discussion section. For the rest of this article, we will refer to the former as “delay-embedding” and the latter as “(MZ) memory effect” “(MZ) memory correction”, or simply “memory” in the figures. Our major aim of the analysis is to compare the performance of the models with delay-embedding and without MZ memory correction to those models with MZ memory correction but without delay-embedding.

We consider the following regression-based models and compared their performance. The first, baseline model is the linear Mori’s projection operator. Our preliminary analysis showed that a direct application of either data-driven Koopman [12] or Mori’s [9] on the set of observables $\{u(\cdot, x_{4i})\}_{i=0}^{31}$ performed poorly [data not reported]. Thus, we adopted the delay-embedding technique [31, 20] to augment the basis functions for learning the MZ kernels based on Mori’s projection operator, which will be referred as “Mori+DEm” model.

Specifically, we use the past H snapshots to augment the input vector (which lives in \mathbb{R}^{32H}). For Mori’s projection operator, we chose $H = 10$. We remark that the lowest-order result of the Mori’s projection operator (i.e., without the higher-order memory corrections, $\mathbf{\Omega}^\ell$, $\ell \geq 1$, in Eq. (5)) is functionally identical to the Hankel-DMD [31]. The second regression-based model was a fully-connected neural network (FCNN). The architecture of the neural network was designed to be two fully-connected layers, each of which contains 32 artificial neurons and a third linear layer with 32 outputs. The third regression-based projection operator was a convolutional neural network (CNN). CNN’s are translationally invariant on the spatially discretized grids; such inductive bias is considered as beneficial for systems like KS equation, which are invariant under translations. The architecture of our designed CNN was two one-dimensional convolutional layers with five channels and kernel size of 11. The circular padding was implemented to impose the periodic boundary condition. The final chosen projection operator for learning MZ memory kernels, we adopted the delay-embedding technique and used $H = 4$ past snapshots as the input for a CNN model, which will be referred as “CNN+DEm” model. In practice, the past H snapshots were stacked in the channel dimension of the input tensor of CNN. The architectures of the delay-embedded CNN model is identical to the one without the delay-embedding.

We used the snapshots collected along the long trajectory with the initial condition u_0^{tr} to learn the MZ kernels $\mathbf{\Omega}^{(\ell)}$ for each regression-based projection operators. For linear projection operators and for FCNN, we applied both the shifting and reordering data augmentation to impose the symmetries. For CNN’s, we applied only the shifting data augmentation. We sampled from the generated test trajectories ($t > t_c$) to perform statistical analyses of the learned regression-based MZ kernels.

As a baseline reference for comparison, we performed reduced-order simulations. In these simulations, the reduced-order snapshots ($\{u_{t,x_{4i}}\}_{i=0}^{31}$) were treated as the full state of the KS-equation discretized on 32 spatially discretized grids (v. 128 of the ground-truth data-generation process). Each of the snapshots was evolved forward in time directly by the ETDRK4 integrator.

In Figure 7, we visualized the predictive trajectories and errors from the learned models, each with $\ell \leq 10$ MZ memory kernels. Figures 7 (b, c) show the spatiotemporal evolution of the reduced-order simulation. Qualitatively speaking, we observed that the reduced trajectory deviated from the “ground-truth” at a prediction horizon ≈ 20 , but it is capable of reproducing dynamical features that are visually indistinguishable. The Mori’s projected model with $H = 10$ delay-embedding (Figs. 7 (d, e)) quickly converged to the mean of the flow as we expected. The FCNN model deviated from the “ground-truth” trajectory sooner than the reduced simulation did, but it also reproduces similar dynamical features; see Figs. 7 (f, g). Predictions from both CNN models Figs. 7 (h-k) deviated later than the reduced simulation did. The $H = 4$ delayed-embedded CNN (Figs. 7 (j, k)) did not significantly improve the plain CNN (Figs. 7 (h, i)).

Quantitative error analysis of the regression models were performed with 15,000 trajectories uniformly sampled on the generated test trajectory. Figure 8 (a) shows the normalized residual of the one-step prediction, defined as the mean squared error of the ℓ^{th} -order MZ model, normalized by that of the Markovian model (i.e., only $\mathbf{\Omega}^{(0)}$). The absolute error values are presented in the inset of Fig. 8 (a). For all the regression models, including the MZ memory reduced the prediction error. We observed that the memory lengths before

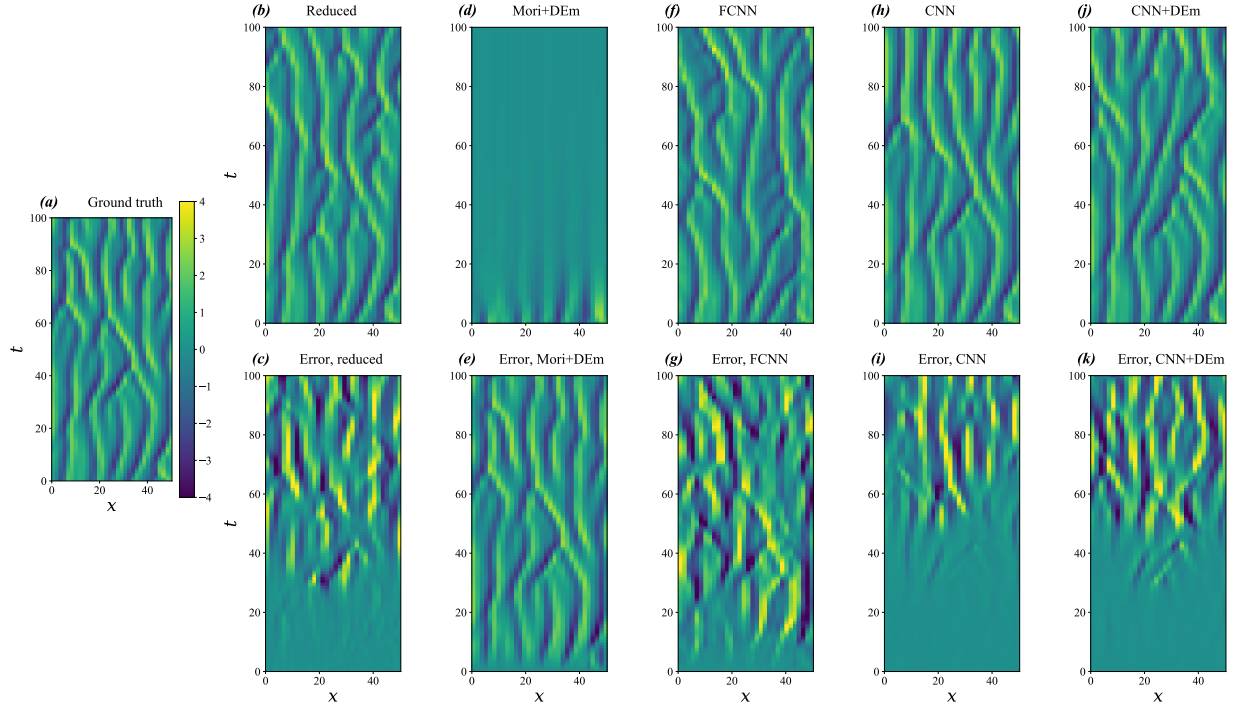


Figure 7: Regression-based Mori-Zwanzig learning of Kuramoto-Sivashinsky system. (a) “Ground-truth” reduced-order observation. (b, d, f, h, j) Predicted trajectories using reduced-order simulation and four regression based Mori-Zwanzig models and (c, e, g, i, k) error of the predicted trajectories. The x - and y -axis of panels (b-k) are identical to those in the panel (a).

the improvement saturated are short for all regression models considered in this numerical experiment. The MZ memory effects can be captured with less than 10 memory kernels. For a reference, the Lyapunov time of the system is ≈ 12.56 [32]. The plain CNN model without delay-embedding showed the highest percentage improvement by including the MZ memory. The delay-embedded CNN model had a slightly smaller percentage improvement in comparison to that of the plain CNN model, despite it has smaller absolute magnitude of mean squared error. This is as expected, as the $H = 4$ delay-embedding is a more expressive model due to its larger input space, allowing coupling the delayed observables. Surprisingly, the plain CNN with $\ell = 4$ MZ contribution has a smaller absolute error than the $H = 4$ delay-embedded CNN; see the Discussion Section for a detailed discussion. The FCNN model exhibited a much larger magnitude of error, and a smaller improvement from MZ memory contributions. Finally, as we expected, the linear Mori's projection operator with delay-embedding had a very poor performance in one-step prediction.

We next focused on predictions at a further horizon. From Fig. 8 (a), we determined the corresponding critical memory lengths for all considered models to be approximately 10. We set the furthest prediction horizon to be 100, which is approximately 8 Lyapunov time. In Figure 8 (b), we compare the mean squared error as a function of the predictive horizon. Similar to the Lorenz '63 system, at short prediction horizon ($\lesssim 20$), models with nonlinear projection operator performed much better than the linear Mori's model. Among the nonlinear models, the FCNN model had worse predictions than the reduced simulation, and both the CNN models out-performed the reduced simulation. Comparing both CNN models, the delay-embedded CNN models performed better than the plain CNN at one-step prediction, as established in Fig. 8 (a). However, the CNN model overtook the time-embedding CNN model and became the best model—in the metric of the mean squared error—among all the considered models before the prediction horizon exceeded 55. As in the Lorenz '63 model, the mean squared error is a less meaningful metric for the long-horizon predictions. As a second metric to quantify model performances, we used the Kullback–Leibler (KL) divergence from the regression-model predicted marginal distribution (u on a single grid) to that of the ground-truth (test trajectory) distribution. Because of the translational symmetry, we accumulated all the measured $u(t, x_{4i}), i = 0 \dots 31$, at different horizons for computing the empirical one-dimensional distributions of u . Figure 8 (c) shows the computed Kullback–Leibler divergence from the predicted distributions at different prediction horizon. Finally, we compared the power spectra of based at the prediction horizon 100; Figure 10 shows the spectrograms of the models. With these metrics, we concluded that the CNN models perform much better than all other models and the reduced simulations over a long prediction horizon. The presented evidence illustrated the advantage of nonlinear projection methods at predicting statistical properties of the dynamical system at a longer prediction horizon, despite the fact that sample-wise, the predicted trajectories deviate from the ground-truth trajectories.

The long-time marginal distribution of the regression-based models and the reduced simulation is shown in Figure 9. The empirical distributions were computed by accumulating measured u on each grid along long predicted trajectories (15,000 steps). The initial conditions of all the models, as well as the reduce simulation, were all set as u_0^{te} . Mori's projection with delay-embedding shows almost δ -like distribution at the mean as expected, while the nonlinear models are capable of reproducing the stationary marginal distribution similar to

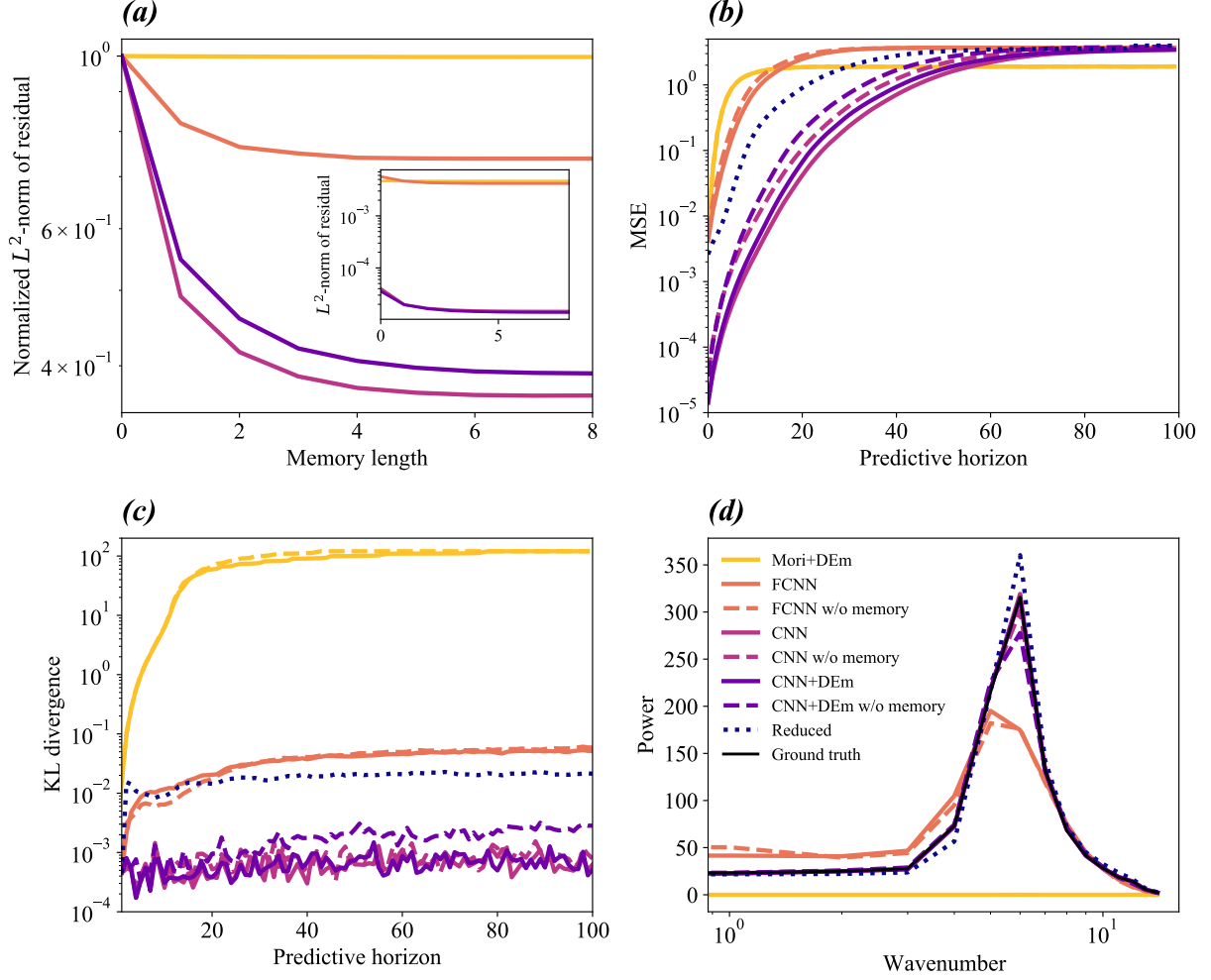


Figure 8: Mori-Zwanzig learning of Kuramoto-Sivashinsky system with regression-based projection operator. (a) The mean squared error of the learned models as a function of memory length. (b) The mean squared prediction error over different prediction horizon. The Lyapunov time for chosen domain size $L = 16\pi$ is approximately 12.56. (c) The Kullback–Leibler divergence of the marginal $(u(t, x_{4i}) \forall i = 0 \dots 31)$ ground-truth distribution from the predicted distribution as a function of prediction horizon. (d) The power spectrum of different models at a prediction horizon 100.

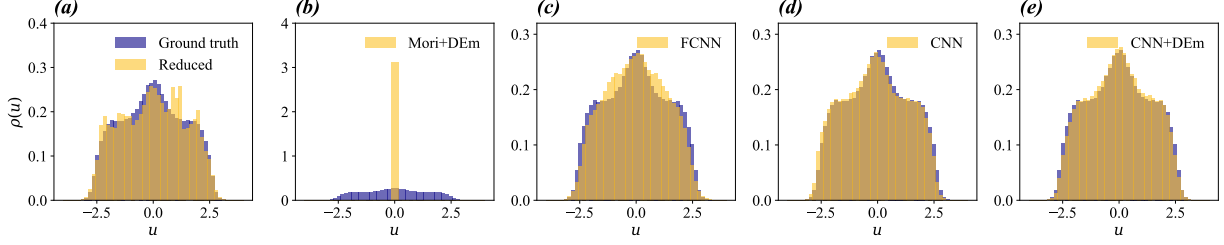


Figure 9: Projection-based Mori-Zwanzig learning of Kuramoto-Sivashinsky system. (a-e) PDFs of long-time predicted trajectories(horizon = 10,000) for five regression-based MZ models.

the “ground-truth”. Among the nonlinear models, the distributions from both CNN models are almost perfectly aligned with that of the test trajectory, while the FCNN model misses the finer details around the mean.

3 Discussion and Conclusion

The central proposition of this article is to adopt the general regression analysis as a projection operator in the Mori–Zwanzig formalism for enabling data-driven learning of dynamical systems. Given a set of pairs of dependent and independent variables, a regression analysis identifies an optimal parametric function of the independent variables, such that the residuals are minimized in some norm, prescribed by the noise model.

In the context of dynamical system, the dependent variables are the future observables, and the independent variables are the present ones. When the system is not fully resolved, sometimes the future observables can not be uniquely determined by the present ones due to missing information of the under-resolved degrees of freedom. Consequently, future observables can be adjective mapping of the present ones, when the system is not fully resolved. A regression projects such adjective mapping to a one-to-one or many-to-one function, depending on the parametric family of the regression model and constrained by the data. Regression is a projection operator because an additional regression analysis on the samples drawn from the best-fit model results in the best-fit model, satisfying the definition of a projection operator $\hat{\mathcal{P}}$: $\hat{\mathcal{P}}^2 = \hat{\mathcal{P}}$.

To identify regression analysis as a projection operator is not a novel idea: it is an established concept in statistics. For example, see [33] for linear regression as an orthogonal projection, and [34] for regularized regression in terms of the Reproducing Kernel Hilbert Space. The notion of the decomposing the samples of the dependent variables into a regressional and an orthogonal component [35] even went back to Kolmogorov in the 1940’s [36]. The major conceptional contribution of this manuscript is the proposition of taking *any* regression analysis as *the* projection operator in the Mori–Zwanzig formalism.

We showed that the special choice of adopting linear regression models results in our previously proposed data-driven learning algorithm for the MZ formalism with Mori’s projection operator [9]. Thus, the proposed regression-based projection operator is a generalization of our previous proposition. Because any regression problem requires the general

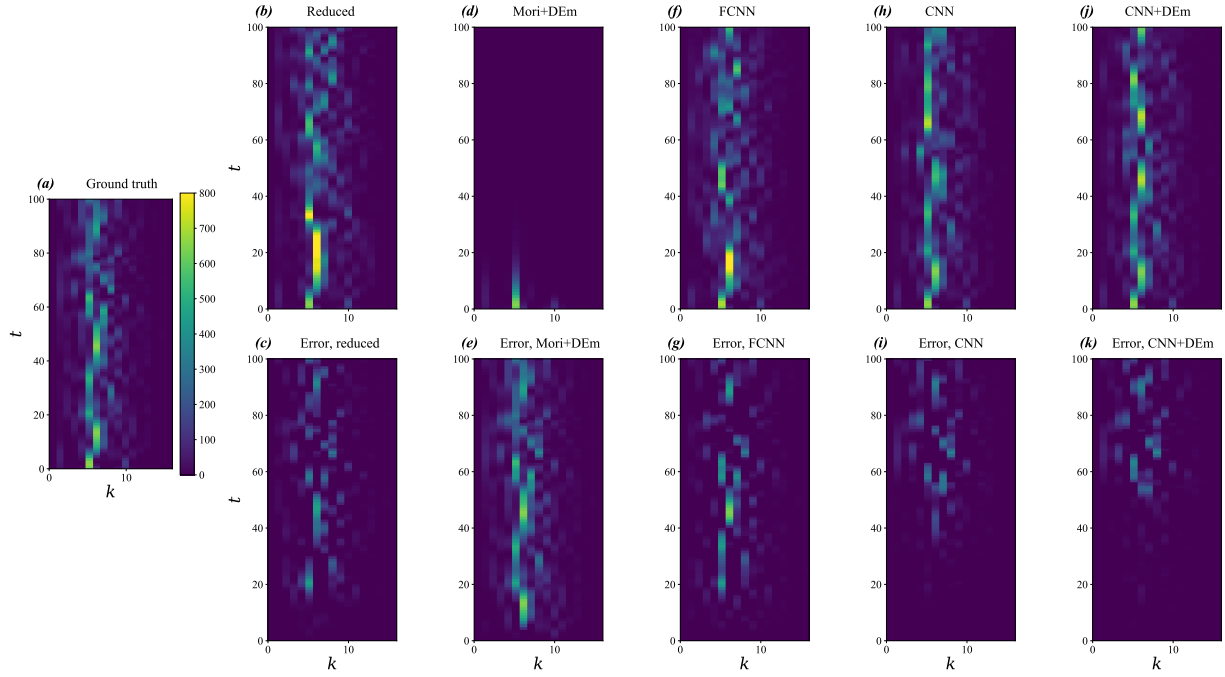


Figure 10: Projection-based Mori-Zwanzig learning of Kuramoto-Sivashinsky system. (a) ”Ground-truth“ spectrum of the coarse-grained trajectory. (b, d, f, h, j) Predicted spectrum using reduced-order simulation and four regression based Mori-Zwanzig models and (c, e, g, i, k) error of the predicted spectrum.

optimization procedure outlined in Eqs. (14)-(17), our proposed procedure to extract the MZ memory kernels is readily applicable to a large set of data-driven learning mechanisms for dynamical systems in the literature. For example, approximate Koopman methods with neural-network-based learning of the functional bases with ridge and sparsity-induced regularizations [18, 19, 20], and Sparse Identification of Nonlinear Dynamics [17, 37]. We remark that these data-driven learning methods often implicitly assume that the system is fully resolved, without missing information. Should it be the case and should the regression model be expressive enough, our iterative procedure would lead to a perfect Markov model $\Omega^{(0)}$ that leaves zero residuals. Our interest, as well as the setup of the whole Mori–Zwanzig formalism, is on partially resolved dynamical systems. In general, when a system is under-resolved and when there exists interaction between the resolved and under-resolved parts of the dynamics, non-negligible orthogonal dynamics (i.e., the residual of the regression) and MZ memory kernels (i.e., $\Omega^{(\ell \geq 1)}$) naturally emerge. The major numerical contribution of this manuscript is to provide a principled algorithm, motivated by the structure of the Generalized Langevin Equation (5), for extracting these higher-order corrections, given any regression model as the projection operator. To the authors’ knowledge, such an intuitive yet elegant procedure does not currently exist in the literature of the Mori–Zwanzig formalism.

Regression-based MZ methods can fill in the gap between the existing Mori’s and Zwanzig’s projection operators, which can be considered as the simplest and the most optimal projection operator [3] respectively. Our proposition significantly broadens practical applicability of the Mori–Zwanzig formalism, because the complexity of the regression model can be gradually adjusted between these two extremes. Ranked by the complexity of the regression analysis, we examined and presented the linear regression analysis on linear functional basis (functionally identical to DMD) or nonlinear functional basis (functionally identical to EDMD), nonlinear polynomial regression, spline regression with ridge regularization as an example of non-parametric regression, and the more modern and expressive neural network architectures such as FCNN and CNN for performing nonlinear regression. With a finite snapshot data set, it may not be computationally feasible to learn the memory kernels with the most optimal Zwanzig’s projection operator, because it requires estimating the conditional expectation functions (e.g, $f(X) := \mathbb{E}[Y|X]$). A finite set of data may not be sufficient to cover all possible condition X , let alone the large amount of samples of Y needed for estimating the expectation value. Instead, regression analysis identifies the best fit among a family of functions to approximate the conditional expectation function. When the family of functions is expressive enough to include the conditional expectation function, our regression-based MZ would converge to the Zwanzig’s projection operator in the infinite-data limit. As neural networks are universal function approximators [38], we hypothesize that the MZ formalism with the optimal Zwanzig projection operator can be reasonably realized by a neural-network-based regression. Indeed, in our numerical experiments, we observed the superiority of those regression models based on neural networks.

We have been framing the above discussions in terms of data-driven learning methods. As a matter of fact, our original desire for developing data-driven MZ methods with nonlinear projection operators emerged from *modeling* reduced-order dynamical systems. Devising closure schemes is not only necessary but also critical in these modeling endeavors. Based on our knowledge, there are few linear closure schemes which resemble the linear projection operators (i.e., approximate Koopman [12, 14] and data-driven Mori [9]). The proposed

MZ formalism with nonlinear regression can connect to existing models in reduced-order models. In the future, we intend to devise nonlinear regression models based on the structure of existing closure schemes. The operational logic is that, despite a purely data-driven (black-box) approach could work, our numerical experiments suggested that this approach is extremely data-hungry. Contrarily, a modeling (white-box) approach requires no data, but only works in a limited scope. We argue the optimal way forward is to use known structures into the learning architecture; with this (grey-box) approach, we are formally injecting inductive biases, which have been pointed out as the critical component for a successful scientific machine learning [39].

In this manuscript, we are primarily interested in the quality of multi-step predictions of reduced-order models. We showed that despite linear regression models out-performed nonlinear ones in the far horizon, it is only because the linear models predicted the mean of the dynamics. Because linear models fully ignore higher-order statistical properties of the dynamical systems, we are not confident that such “coarse-grained dynamical systems” are the proper way forward for making predictions. Although such a problem for linear projection operator does not exist when a set of observables linearly spanned an invariant Koopman space, it is very difficult to identify the set in practice. It is our perspective that developing nonlinear projection operator methods is a more promising way forward for predictive coarse-grained models. We do remark that methods based on linear projection operators are ideal in estimating the Koopman eigenvalues and eigenfunctions, and the learning problem is easier: it is globally convex provided a set of linearly independent observables. We should remark that nonlinear regression is not always advantageous in making predictions. As we witnessed in the Lorenz ‘63 model, despite a learned nonlinear regression model could improve predictive accuracy within a finite horizon, sometimes these nonlinear closure methods lost long-term stability (Fig. 5). Such a pathology is model- and horizon- dependent and interestingly, not observed when we used neural-network-based regression.

On the Kuramoto–Sivashinsky model, we also compared the delay-embedding and the memory effect of the Mori–Zwanzig formalism. Our motivation was to provide a clear clarification on a pervasive confusion between these two memory-dependent theories, and to provide numerical results on respective data-driven learning methods. Such a confusion emerged from a false presumption that all memory-dependent theories are equivalent.

As the memory effect in Mori–Zwanzig formalism is due to the interaction between the resolved and under-resolved dynamics, the memory kernels and the orthogonal dynamics must satisfy the stringent Generalized Fluctuation Dissipation Relationship (Eq. (10)), which depends on the choice of the projection operator \mathcal{P} . Notably, the MZ memory contribution is always a linear sum of memory kernels evaluated at each past snapshot (Eq. (5)). There exists no cross terms—e.g., some nonlinear function f coupling observations at two times $f(\mathbf{g}_t \circ \phi_0, \mathbf{g}_{t-1} \circ \phi_0)$ —in the MZ formalism because the projection operator \mathcal{P} is applied at each discrete time by construction. The functional space that \mathcal{P} is projected into is those regressional functions f_θ , whose domain is M reduced-order observables at an instantaneous time.

On the contrary, for delay-embedding, the domain of the functions is augmented to include H past snapshots of M reduced-order observables. The motivation of delay-embedding is that the past history may contain useful information for inferring the under-resolved dynamics. Because such an augmented functional space ($M \times H$) is larger than the fixed (M)

operational space in the Mori–Zwanzig formalism, delay-embedding can be considered as a more expressive regression model. Let us denote the past H snapshots of the observables $\mathbf{g}_{t,t-1\dots t-H+1} \circ \phi_0$ by a flattened vector $\mathbf{g}_{t-H+1:t} \in \mathbb{R}^{HM}$. Formally, delay embedding can be considered as a regression to identify the optimal function $\mathbf{f}_{\theta^*}(\mathbf{g}_{t-H+1:t})$ that best approximates \mathbf{g}_{t+1} . As such, cross terms ($f(\mathbf{g}_t \circ \phi_0, \mathbf{g}_{t-1} \circ \phi_0)$) could exist, should the family of regressional functions admits, with the delay-embedding paradigm. Hankel-DMD [31] is the special delay-embedding case that the learning is formulated as a linear regression problem, i.e., the regressional functions take the form $\mathbf{f}_{\theta}(\mathbf{g}_{t-H+1:t}) := \boldsymbol{\theta}^T \cdot \mathbf{g}_{t-H+1:t}$. Although its structure resembles Mori–Zwanzig’s Generalized Langevin Equation with Mori’s linear projection operator, it is not necessary—and generally not the case—that the best-fit parameters of the Hankel DMD satisfy the Generalized Fluctuation-Dissipation relation 10.

We know that the structure of Generalized Langevin Equation is contained in the family of regressional functions in the delay-embedded CNN, the error of the latter should have been lower-bounded by that of the former. Our numerical result that the Mori–Zwanzig formalism with $\ell < 4$ memory contribution out-performed the more expressive delay-embedded CNN with $H = 4$ highlights the practical difficulty of learning larger nonlinear regression models: they require more data, and in nonlinear regression, the training could be trapped in some local minima of the cost function. We also observed a much worse multi(> 1)-step prediction by delay-embedded model, compared to Mori-Zwanzig formalism. We hypothesize one cause could be the error from the neglected orthogonal dynamics \mathbf{W}_t only contributes to one prediction at $t + 1$ in the Mori–Zwanzig formalism, but the error would contribute directly to H predictions forward ($t + 1$ to $t + H$) with the delay embedding.

Interestingly, Mori–Zwanzig formalism and delay embedding are not mutually exclusive. On the Kuramoto–Sivashinsky model, we also examined a delay-embedded CNN with Mori–Zwanzig memory kernels. In this combined approach, the Markov term would be a vector function of the flattened vector $\mathbf{g}_{t-H+1:t}$, and the ℓ th-order ($\ell \geq 1$) memory kernel would be a vector function of the flattened vector $\mathbf{g}_{t-H-\ell+1:t-\ell}$. We concluded that the inclusion the the Mori–Zwanzig memory kernels can further improve the performance of the delay-embedded CNN.

We viewed regression-based Mori–Zwanzig formalism as a promising direction to enable data-driven learning for partially observed dynamical systems. We identified a few directions which merit further investigation. Theoretically, we would like to generalize the formalism for stochastic systems, including generic stochastic processes, Hidden Markov Models, and random dynamical systems. As an application, we are working on the application of the NN-based Mori–Zwanzig models on isotropic turbulence data [10]. Finally, in this manuscript, we did not attempt to model the orthogonal dynamics, which is needed for making accurate predictions. Our test showed that the common choice of white (independent in time) Gaussian noise is unsatisfactory [data not shown]. A certain color-noise must be needed, as the orthogonal dynamics, which are just the under-resolved dynamics, are also correlated in time. Despite that our numerical extraction of the orthogonal dynamics provides the data stream for learning, how one models the the orthogonal dynamics in a principled and system-agnostic way remains an open and challenging problem.

Author contributions

YTL conceived and performed the theoretical developments. YT and YTL performed the numerical analysis. YTL, YT, and DL contributed equally in designing the numerical analysis and writing the manuscript.

Acknowledgement

This project was primarily supported by the Laboratory Directed Research and Development (LDRD) Project “Uncertainty Quantification for Robust Machine Learning” (20210043DR). YT and YTL were also partially supported by the LDRD project “Accelerated Dynamics Across Computational and Physical Scales” (20220063DR).

References

- [1] Mori H. Transport, Collective Motion, and Brownian Motion. *Progress of theoretical physics*. 1965;33(3):423-55.
- [2] Zwanzig R. Nonlinear Generalized Langevin Equations. *Journal of Statistical Physics*. 1973;9(3):215-20.
- [3] Alexandre J Chorin, Hald OH, Kupferman R, Chorin AJ, Hald OH, Kupferman R. Optimal Prediction with Memory. *Physica D: Nonlinear Phenomena*. 2002 Jun;166(3-4):239-57.
- [4] Okamura M. Validity of the essential assumption in a projection operator method. *Physical Review E*. 2006;74(4):046210.
- [5] Mori H, Okamura M. Dynamic structures of the time correlation functions of chaotic nonequilibrium fluctuations. *Physical Review E*. 2007;76(6):061104.
- [6] Meyer H, Pelagejcev P, Schilling T. Non-Markovian out-of-equilibrium dynamics: A general numerical procedure to construct time-dependent memory kernels for coarse-grained observables. *EPL (Europhysics Letters)*. 2020;128(4):40001.
- [7] Maeyama S, Watanabe TH. Extracting and modeling the effects of small-scale fluctuations on large-scale fluctuations by Mori–Zwanzig projection operator method. *J Phys Soc Jpn*. 2020;89(2):024401.
- [8] Meyer H, Wolf S, Stock G, Schilling T. A numerical procedure to evaluate memory effects in non-equilibrium coarse-grained models. *Adv Theory Simul*. 2021;4(4):2000197.
- [9] Lin YT, Tian Y, Livescu D, Anghel M. Data-Driven Learning for the Mori–Zwanzig Formalism: A Generalization of the Koopman Learning Framework. *SIAM Journal on Applied Dynamical Systems*. 2021 Jan;20(4):2558-601.
- [10] Tian Y, Lin YT, Anghel M, Livescu D. Data-Driven Learning of Mori–Zwanzig Operators for Isotropic Turbulence. *Physics of Fluids*. 2021 Dec;33(12):125118.

- [11] Rowley CW, Mezić I, Bagheri S, Schlatter P, Henningson DS. Spectral Analysis of Nonlinear Flows. *Journal of Fluid Mechanics*. 2009;641:115-27.
- [12] Schmid PJ. Dynamic Mode Decomposition of Numerical and Experimental Data. *Journal of Fluid Mechanics*. 2010;656:5-28.
- [13] Schmid PJ, Li L, Juniper MP, Pust O. Applications of the Dynamic Mode Decomposition. *Theoretical and Computational Fluid Dynamics*. 2011 Jun;25(1):249-59.
- [14] Williams MO, Rowley CW, Kevrekidis IG. A Data-Driven Approximation of the Koopman Operator : Extending Dynamic Mode Decomposition. *Journal of Nonlinear Science*. 2015;25(6):1307-46.
- [15] Durbin P. Some recent developments in turbulence closure modeling. *Annual Review of Fluid Mechanics*. 2018;50:77-103.
- [16] Majda AJ, Wang X. Nonlinear dynamics and statistical theories for basic geophysical flows. Cambridge University Press; 2006.
- [17] Brunton SL, Proctor JL, Kutz JN. Discovering governing equations from data by sparse identification of nonlinear dynamical systems. *Proceedings of the National Academy of Sciences*. 2016;113(15):3932-7.
- [18] Li Q, Dietrich F, Bollt EM, Kevrekidis IG. Extended Dynamic Mode Decomposition with Dictionary Learning: A Data-Driven Adaptive Spectral Decomposition of the Koopman Operator. *Chaos: An Interdisciplinary Journal of Nonlinear Science*. 2017 Oct;27(10):103111.
- [19] Yeung E, Kundu S, Hodas NO. Learning Deep Neural Network Representations for Koopman Operators of Nonlinear Dynamical Systems. 2019 American Control Conference (ACC). 2017:4832-9.
- [20] Lusch B, Kutz JN, Brunton SL. Deep Learning for Universal Linear Embeddings of Nonlinear Dynamics. *Nature Communications*. 2018;9(1).
- [21] Lin KK, Lu F. Data-Driven Model Reduction, Wiener Projections, and the Koopman-Mori-Zwanzig Formalism. *Journal of Computational Physics*. 2021 Jan;424:109864.
- [22] Gerlich G. Die Verallgemeinerte Liouville-Gleichung. *Physica*. 1973 Nov;69(2):458-66.
- [23] Zwanzig R. Nonequilibrium Statistical Mechanics. Mm. Oxford University Press; 2003.
- [24] Darve E, Solomon J, Kia A. Computing Generalized Langevin Equations and Generalized Fokker-Planck Equations. *Proceedings of the National Academy of Sciences*. 2009 Jul;106(27):10884-9.
- [25] Koopman BO, v Neumann J. Dynamical Systems of Continuous Spectra. *Proceedings of the National Academy of Sciences*. 1932;18(3):255-63.

- [26] Lorenz EN. Deterministic Nonperiodic Flow. *Journal of Atmospheric Sciences*. 1963;20(2):130-41.
- [27] Kuramoto Y. Diffusion-Induced Chaos in Reaction Systems. *Progress of Theoretical Physics Supplement*. 1978 Feb;64:346-67.
- [28] Sivashinsky GI. On Flame Propagation under Conditions of Stoichiometry. *SIAM Journal on Applied Mathematics*. 1980;39(1):67-82.
- [29] Sivashinsky GI. Nonlinear Analysis of Hydrodynamic Instability in Laminar Flames—I. Derivation of Basic Equations. *Acta Astronautica*. 1977;4(11):1177-206.
- [30] Kassam AK, Trefethen LN. Fourth-Order Time-Stepping for Stiff PDEs. *SIAM Journal on Scientific Computing*. 2005 Jan;26(4):1214-33.
- [31] Arbabi H, Mezić I. Ergodic Theory, Dynamic Mode Decomposition, and Computation of Spectral Properties of the Koopman Operator. *SIAM Journal on Applied Dynamical Systems*. 2017;16(4):2096-126.
- [32] Edson RA, Bunder JE, Mattner TW, Roberts AJ. Lyapunov Exponents of the Kuramoto–Sivashinsky PDE. *The ANZIAM Journal*. 2019;61(3):270-85.
- [33] Deisenroth MP, Faisal AA, Ong CS. *Mathematics for Machine Learning*. Cambridge University Press; 2020.
- [34] Nosedal-Sanchez A, Storlie CB, Lee TC, Christensen R. Reproducing kernel Hilbert spaces for penalized regression: A tutorial. *The American Statistician*. 2012;66(1):50-60.
- [35] Afriat SN. In: Fox KA, Sengupta JK, Narasimham GVL, editors. *Regression and Projection*. Berlin, Heidelberg: Springer Berlin Heidelberg; 1969. p. 277-301.
- [36] Kolmogorov AN. On the proof of the method of least squares. *Uspekhi Mat Nauk*. 1946;1(1 (11)):57-70.
- [37] Kaheman K, Kutz JN, Brunton SL. SINDy-PI: a robust algorithm for parallel implicit sparse identification of nonlinear dynamics. *Proceedings of the Royal Society A: Mathematical, Physical and Engineering Sciences*. 2020;476(2242):20200279.
- [38] Murphy KP. *Machine Learning: A Probabilistic Perspective*. MIT press; 2012.
- [39] Lu L, Jin P, Pang G, Zhang Z, Karniadakis GE. Learning Nonlinear Operators via DeepONet Based on the Universal Approximation Theorem of Operators. *Nature Machine Intelligence*. 2021 Mar;3(3):218-29.